CRYSTALLIZATION-DRIVEN SELF-ASSEMBLY OF HYDROLYTICALLY-DEGRADABLE BLOCK POLYMERS INTO DIVERSE NANOSTRUCTURES

A Thesis

by

JESSICA HIN HUANG

Submitted to the Office of Graduate and Professional Studies of
Texas A&M University
in partial fulfillment of the requirements for the degree of

MASTER OF SCIENCE

Chair of Committee,	Karen L. Wooley
Committee Members,	Brian Applegate
	Janet Bluemel
	David C. Powers
Head of Department,	Simon W. North

December 2018

Major Subject: Chemistry

Copyright 2018 Jessica Huang

ABSTRACT

Cysteine-functionalized poly(L-lactide)-*block*-polycarbonates (PLLA-*b*-PC-cys) were synthesized and assembled in nanopure water, by crystallization-driven self-assembly (CDSA), to yield a variety of nanostructures, of which the dimensions were determined by the polymer composition. CDSA exploits crystallization of one segment of a block polymer to trap nanoscale morphologies that are inaccessible by solution-state self-assembly. This project expands the scope of CDSA-mediated block polymer nanostructures by the design, synthesis, and assembly of fully-degradable PLLA-*b*-PC, in which the semi-crystalline polylactide block enables CDSA and the polycarbonate block contains alkyne groups for post-polymerization modification. Installation of zwitterionic cysteine moieties onto the polycarbonate alkynes rendered the block polymers amphiphilic. CDSA was performed in nanopure water, by heating above the T_g of the PLLA block and cooling to induce assembly. The morphology of the resulting nanostructures was investigated as a function of block length and ratio by atomic force microscopy (AFM).

These studies demonstrated that spherical, cylindrical, or platelet-like morphologies could be generated, depending on the ratio of the hydrophobic block to the hydrophilic block. Polymers with hydrophobic weight percentages lower than 30% formed only spheres, while assembly of those with intermediate weight percentages (34% and 36%) resulted in platelets with lengths of *ca.* 500 nm. Finally, polymers with the highest weight percentages (42% and 71%) yielded large bundles of cylinders, *ca.* 500 nm or longer.

Reproducible assembly of a fully-degradable polymeric system is a significant step towards drug delivery applications. The polymer assemblies described in this thesis are currently under investigation as tunable delivery vehicles for silver antimicrobials to treat recurrent urinary tract infection (UTI).

ACKNOWLEDGEMENTS

I would like to thank my committee chair, Dr. Karen L. Wooley. I am grateful for not only her guidance, but also her generosity. I would also like to thank my committee members, Dr. Brian Applegate, Dr. Janet Bluemel, and Dr. David C. Powers, for their kind support throughout my time here.

Thanks also go to my friends and colleagues and the department faculty and staff. Valuable scientific discussions with Mei Dong, Simcha E. Felder, Dr. Rachel A. Letteri, Yen-Nan Lin, Yue Song, and Hai Wang are particularly appreciated. Further gratitude goes to Dr. Rachel A. Letteri, for the generous editing of this document and her kind leadership in the group. Additionally, special acknowledgment goes to Sandy Horton, Academic Advising Program Coordinator of the chemistry department, for her compassionate support. This work would not be possible without these people.

Finally, thanks go to my mother and father, Linda Polam Lee Huang and Fuping Huang, for their support and love throughout my life, and, to Dr. Jake A. Boissonnault, for his exceeding patience and kindness.

CONTRIBUTORS AND FUNDING SOURCES

Contributors

This work was supported by a thesis committee consisting of Professors Karen L. Wooley (advisor), Janet Bluemel, and David C. Powers of the Department of Chemistry, and Professor Brian Applegate of the Department of Biomedical Engineering.

The IR spectroscopy, TGA, DSC, and AFM data were collected by the student in the Texas A&M Laboratory for Synthetic-Biologic Interactions (LSBI) facility. All other work conducted for the thesis was completed by the student independently.

Funding Sources

This work was made possible in part by the National Science Foundation under Grant Number DMREF-1629094 and the Robert A. Welch Foundation through the W. T. Doherty-Welch Chair in Chemistry under Grant Number A-0001. Its contents are solely the responsibility of the author and do not necessarily represent the official views of the National Science Foundation or the Robert A. Welch Foundation.

TABLE OF CONTENTS

Page

LIST OF FIGURES

Page

LIST OF TABLES

Page

INTRODUCTION

Overview and motivation

Nanoparticles are attractive for drug-delivery purposes due to the potential for high drug loading, increased bioavailability of hydrophobic active pharmaceutical ingredients (API), and increased stability of drugs upon loading into nanoparticles.[1-2] Specifically, nanoparticles with an intermediate size (20-100 nm) are especially well tolerated by the body's natural circulation, clearance, tissue distribution, and intracellular response mechanisms. Due to their sub-micron size, nanoparticles can use fine capillaries to penetrate deep into tissues, cross the fenestration of epithelial linings, and enter cells.[1] Additionally, due to their high aspect ratio, cylindrical nanoparticles typically exhibit longer *in vivo* circulation times[3] and access alternative cell internalization pathways[4] relative to spherical nanoparticles. Furthermore, nanoparticles offer multiple advantages over typical (*e.g.* tablet, capsule, extended release) formulations in that the size, shape, and chemical composition can be precisely tailored to target cells and tissues, respond to external stimuli, and display tunable optoelectronic and diagnostic/theranostic properties.[5]

For polymers designed for biomedical applications, degradability is a key advantage, alleviating concerns related to long-term accumulation in the body. To this end, our group has prepared nanoparticle-based drug-delivery vehicles by assembly of glucose-based polycarbonates[6-8] and polyphosphoesters,[9] among others. Crystallization-driven self-assembly (CDSA) enables construction of nanoparticles with controllable dimensions by crystallization and trapping of non-equilibrium morphologies. Block polymers with a degradable and semi-crystalline poly(L-lactic acid) (PLLA) hydrophobic component have been successfully assembled by crystallization-driven self-assembly (CDSA) into nanoparticles, but this has mainly been

demonstrated in materials with non-degradable hydrophilic blocks.[10-11] Recently, our laboratory reported the synthesis and CDSA of fully degradable block polymers of PLLA and a glucose-based polycarbonate with a relatively high T_g (64 °C as a alkyne-functionalized diblock with PLLA; and 114 °C as a cysteine-functionalized diblock with PLLA), attributed to its relative stiffness and steric bulk that decreases flexibility and prevents rearrangement of the backbone.[6, 12] In this work, the synthesis and CDSA of a polymer comprised of semicrystalline PLLA and a more flexible, aliphatic polycarbonate, with a lower T_g (-4 - 22 ºC as an alkyne-functionalized diblock) is investigated. The more flexible backbone provides an opportunity to further tune assembly morphology and degradation within a fully-degradable amphiphilic block polymer platform.

In this introduction, a background on polymers and ring-opening polymerizations, polylactides, polycarbonates, functionalization of polymers by click chemistry, and strategic utilization of the glass transition temperature, self-assembly, and crystallization-driven self-assembly will be presented.

Polymers

Polymers are macromolecules consisting of many units, where chemical bonds connect smaller repeating units called monomers.[13] Those that are synthesized by living organisms are called biopolymers, including cellulose, lignin, and DNA. Polymers comprised of only one type of repeating unit are called homopolymers, whereas those with two or more different types of repeating unit are called copolymers. The resulting architecture can be linear or more complex structures, such as brushes, stars, and dendrimers.

One of the ways that polymers can be characterized is by molar mass and degree of polymerization.[13] The molar mass of a homopolymer $M = xM_0$, where M is the molar mass, x is the number of repeat units, and M_0 is the weight of each repeat unit. The ratio M_w / M_n is known as the dispersity of the polymer, $Đ$. Typically, polymers have a range between $Đ$ = 1.5-2.0, though controlled polymerizations yield polymers with narrow dispersity $Đ < 1.2$. A perfectly monodisperse polymer would have $Đ = 1.00$.

Syntheses of polymers have two different types – step growth and chain growth. In step growth polymerization, the polymer chains grow between two molecular species in a stepwise fashion – for example, a monomer reacting with a monomer to yield a dimer, two dimers forming a tetramer, a tetramer adding a monomer to yield a pentamer – to yield a polymer. Conversely, in chain growth polymerization, the polymer chains grow only by reaction of monomer on the active chain end.

In some cases, it is possible to conduct polymerizations without inadvertent chain end termination or chain transfer, such that the active chain ends continue to react in a controlled manner with monomer until the monomer supply is exhausted. In these cases, the rate of initiation is much higher than the rate of propagation, and the polymerization is considered to be "living." Living polymerizations, such as the controlled ring-opening polymerizations described next, give access to materials with narrow molar mass distributions ($Đ < 1.2$).[13]

Ring-opening polymerization

Ring opening polymerization is a living chain-growth polymerization, in which the terminal end of a ring-opened monomer reacts further with other cyclic monomers by ring-opening.[14-16] Polymers with the general structure -[-R-Z-]$_n$-, where Z is a linking group such as an ether, ester, or amide, can be prepared by either step growth polycondensation of bifunctional

linear molecules or by chain growth ring-opening polymerization of the corresponding cyclic R-Z molecule. The driving force for the ring-opening of cyclic monomers is dependent on three different factors: ring strain, conformation, and steric repulsion between atoms crowded into the center of the ring.[17] Therefore, as for other polymerizations, the net enthalpy of the process is negative. The enthalpy of polymerization for smaller cyclic molecules – such as 3-membered or 4-membered lactones – is considerably higher than that of 5-, 6-, or 7-membered lactones; therefore, the latter are more energetically costly to ring-open. In fact, ring-opening polymerizations of 5-membered lactones often require high pressure to afford moderate yields.[18-20] Typically, these kinds of ring-opening reactions require a catalyst, such as an acid or base.[13]

Drug delivery applications often require well-defined materials to circumvent concerns of different mechanisms of actions from polymers with different molecular weights. During polymerization, chain transfer events, or reactions that terminate the active chain end and activate another moiety elsewhere on the chain or on the solvent or other reagent may occur, generating broad molar mass distributions. To ensure living ROP, the catalyst must exhibit a negligible rate constant for transesterification reactions involving the polymer backbone.

For ROP to yield materials designed for medical applications, there has been considerable value placed on metal-free organic catalysts, as many of the metals used to catalyze ROP are undesirable for use in the body. In metal-free catalysis, the replacement of basic (-)-sparteine with other tertiary amines accelerated ROP, due to the increased basicity of the so-called "superbases": 1,5,7-Triazabicyclo[4.4.0]dec-5-ene (TBD), *N*-methyl-TBD (MTBD), and 1,8-diazabicyclo[5.4.0]- undec-7-ene (DBU) were shown to be effective organocatalysts for the ring-opening polymerization (ROP) of cyclic esters such as lactide (LA), δ-valerolactone (VL), and ε-caprolactone (CL).[21] VL and CL can be polymerized by TBD alone, whereas DBU and

MTBD can only polymerize these monomers in the presence of a thiourea co-catalyst. In organocatalyzed ROP, no catalyst is incorporated into the polymer and the end group is determined by the alcoholic initiator and the non-initiating end of the polymer. As the most active of these three organocatalysts, TBD was selected for the polymerizations of lactide and cyclic carbonates described in this thesis. Advantages of functional cyclic carbonate monomers, such as the PC-alkyne in this work, include their amenability to living polymerizations, which produce narrow molar mass dispersity, the hydrolytic degradability of the resulting polymers for potential use as a drug delivery vehicle or other bioapplications, and versatile functional groups (for example, an alkyne handle) that allows various post-polymerization click reactions.

Aliphatic polycarbonates (PC)

Aliphatic polycarbonates are promising as biomaterials because of their biodegradability, biocompatibility, and low toxicity. They were shown to undergo slow hydrolytic degradation under physiological conditions *in vitro* and accelerated enzymatic degradation *in vivo*: a poly(trimethylene carbonate) (TMC) film exhibited 9% weight loss over 30 weeks *in vitro via* hydrolytic degradation, while the film exhibited 21% weight loss over 24 weeks in rats.[22] The degradation products are derivatives of propane-1,3-diol and carbon dioxide, which are considered relatively harmless to biological systems. The development of organocatalytic systems, such as DBU and TBD, allowed for metal-free synthesis of poly(TMC). TBD yielded quantitative conversion of monomer within minutes, where the degree of polymerization was easily controlled by altering the ratio of monomer to initiator. The short reaction time, robustness of the polymerization, and narrow dispersion makes this polymerization ideal for replicating polymeric samples with the same chemical and physical properties.

Poly(lactide) (PLA)

Poly(lactide), known as PLA, has had a long history of safety in humans and an extensive range of applications.[23-24] It is biocompatible, biodegradable by both hydrolytic and enzymatic mechanisms, displays a large range of mechanical and physical properties that can be engineered to suit multiple applications, and has low immunogenicity. Formulations containing PLA have been Food and Drug Administration (FDA)-approved, which is a further incentive for PLA-based materials for expedited clinical translatation.[25] Lactide exists as two optical forms, namely D-lactide and L-lactide. A semicrystalline polymer of poly(L-lactide) is obtained from L-lactide and is a hard transparent polymer with a tensile strength of 45-70 MPa, while racemic poly(DL-lactide) (PDLLA) is amorphous with no melting point and lower tensile strength of 28-50 MPa.[24, 26]

Click functionalization

Click reactions provide a highly efficient, versatile set of methods for functionalization of polymers.[27] In particular, two types of click chemistry are widely-used for modifying polymers: copper(I)-catalyzed alkyne-azide cycloaddition and photo-initiated thiol-ene/thiol-yne reactions. In 2001, Sharpless, *et al*, coined the term "click chemistry" to refer to a set of efficient reactions that couple small building blocks *via* heteroatom-containing linkages. Such reactions should be modular, high-yielding, and generate only relatively harmless side products, and require mild reaction conditions.[28] Several well-known click reactions include: the hetero-Diels-Alder reaction, thiol-ene or thiol-yne coupling, the Staudinger ligation, native chemical ligation, sulfo-click, and copper-catalyzed alkyne-azide cycloaddition (CuAAC).[28]

Thiol-ene and thiol-yne reactions involve UV-catalyzed homolytic addition of a thiol radical to alkenes or alkynes. The first report was in 1949 with thioacetic acid as the thiol-

containing reagent[29-30], and the reaction could be accelerated in some cases using UV photoirradiation and addition of peroxide-forming radical initiators such as ascaridole. The reaction was rediscovered in 2009 as a route to highly crosslinked networks.[31] Currently, the thiol-yne addition mechanism is used as a convenient reaction for post-polymerization modification of polymers with pendant alkyne groups, placing two reactive thiols on each alkyne-bearing unit.[32-33] Click reactions are particularly useful for post-polymerization functionalization with hydrophilic thiols to render block polymers amphiphilic, as charged groups are incompatible with many controlled polymerization techniques yielding degradable polymers (*e.g.*, ROP). Our group has used this technique to modify alkyne and alkyne containing degradable polymers to render them amphiphilic.[6-7, 9, 12] Using organic radical initiators such as 2,2-dimethoxy-2-phenylacetophenone (DMPA) renders these click reactions metal-free, which is particularly important for polymers designed to complex metals (for example, silver for antimicrobial applications).

Glass transition temperature

When designing block polymers for CDSA, the glass transition is of vital importance, as the block controlling the CDSA must be heated above T_g to access the rubbery state, in which the chains have increased mobility and therefore an enhanced ability to rearrange and assemble. The glass transition is the temperature range in which a polymer transitions from a glass to a rubber.[13] Any material that can be cooled significantly below its melting temperature without crystallizing will exhibit a glass transition, unless plasticizing agents such as water are in the system. Below the glass transition, the polymer is stiff and glassy, and other physical properties such as heat capacity and thermal expansion coefficient are also affected.

Common ways to determine T_g include dilatometry, thermomechanical analysis (TMA), dynamic mechanical analysis (DMA), and differential scanning calorimetry (DSC). Dilatometry determines T_g by measuring the specific volume of a polymer sample as a function of temperature. Upon heating beyond the T_g, the rubbery polymer chain occupies more free volume than do the glassy polymer chains.[34] TMA determines T_g by using a mechanical probe to measure the expansion of the polymer as a function of temperature. Above the T_g, a sharp increase in volume is observed. In DMA, the response of the material to applied stress is determined as a function of temperature and the T_g is noted as the temperature range in which the modulus changes appreciably. Perhaps the most common method to determine T_g is by DSC, where heating above the T_g leads to an increase in heat capacity of the polymer. Notably, T_gs are dependent upon the heating rate and other conditions of the measurement.

When designing block polymers, multiple factors that influence the glass transition temperature are considered, including chemical structure, molar mass, and composition.[35] One of the primary factors is monomer structure. Polymers with relatively low T_g (below room temperature) are called elastomers; elastomers can be crosslinked into permanent networks, where their elasticity is employed in rubber bands, O-rings, gaskets, and tires. Polymers with T_g at around 100 °C or above are considered thermoplastics, as they can be processed above the T_g and solidified to plastic parts upon cooling to room temperature. Additionally, T_g increases with backbone rigidity, presence of rigid or sterically bulky side groups, and weak intermolecular interactions; all of these reduce polymer chain motion. Incorporation of low molar mass polymers or a polymeric component with a lower T_g can reduce T_g.

PLLA exhibits a glass transition at *ca.* 55-60 °C,[10] while PLLA-based diblock polymers have been shown to exhibit either an intermediate T_g, or two T_gs, if both blocks exhibit a T_g. If

the two blocks are well-mixed, an intermediate T_g will be observed. If they segregate into distinct domains, for instance, into a PLLA-rich region, and a PLLA-poor region, two T_gs will be observed.[36] For instance, in blends of PLLA and PDLLA- PGA_{50} (composition ratio of PDLLA and polyglycolide (PGA) 50 : 50), the T_g decreased from that of PLLA (about 58 °C) to that of PDLLA- PGA_{50} (*ca.* 30 °C).[37] The Fox equation (**Equation 1**) is a simplified expression derived from the thermodynamics of a mixture of two components, such as a polymer mixed with low molar mass compounds, a blend of two polymers, or a statistical copolymer.[35] Assuming that the specific heats and glass transition temperatures of the two components are similar; the Fox equation agreement with the observed transitions is generally very good.[35]

To enable CDSA, block polymers must undergo a moderately high glass transition at least above room temperature, so that the polymers are able to rearrange due to its rubbery state. When finished assembling, the assemblies can be cooled below its T_g to lock the morphology.

Macromolecular self-assembly in solution

Typically, self-assembly of amphiphilic block polymers into nanostructures occurs in a selective solvent.[38] Generated nanostructures include spherical micelles, vesicles (polymersomes), cylinders/rods, lamellae, bicontinuous structures, large compound micelles, and disc-like micelles among others. The driving force for self-assembly in selective solvents is the minimization of thermodynamically unfavorable interactions, for example between water and the hydrophobic block of an amphiphilic block copolymer. The size and structure of the generated nanostructures are also impacted by steric and electrostatic repulsion, where applicable, between the soluble blocks in the selective solvent.[39]

The simplest and most common nanostructure formed from block polymers in solution is the spherical micelle.[38] Briefly, the thermodynamic assembly of amorphous diblock polymers is

dependent on the volume fraction of each block. As volume fraction of the hydrophobic block A (f_A) increases, the morphology of the resulting nanostructures changes from spheres, to cylinders, to bilayered structures and lamellae. Typically, hydrophilic to hydrophobic ratios greater than 1:1 v/v form micelles; copolymers with a ratio less than 1:2 form vesicles; those with ratios less than 1:3 may form vesicles, inverted micro structures, other complex structures, and finally macroscopic precipitates.[40]

For block polymers with a glassy hydrophobic block (*i.e.*, with a T_g above room temperature), kinetic quenching may be performed using a co-solvent to kinetically trap desired morphologies. The amphiphilic block polymers are dissolved in a non-selective solvent (literature examples include dimethylformamide (DMF), tetrahydrofuran (THF), or dioxane), and a selective solvent (such as water) is slowly added into the solution to access kinetic morphologies as desired, then quenching with an excess amount of water, which freezes kinetic processes and morphologies.[41]

$$\frac{1}{T_g} = \frac{w_1}{T_{g,1}} + \frac{w_2}{T_{g,2}}$$

Equation 1. Fox equation describing the glass transition of polymer blends, where T_g is the glass transition temperature of the mixture, w_1 and w_2 are the weight fractions of the two components, respectively, and $T_{g,1}$ and $T_{g,2}$ are the glass transition temperatures of the two components, respectively.

Crystallization-driven self-assembly

Amphiphilic block polymers are capable of self-assembly into macromolecular nanostructures, where the hydrophilic blocks face outwards, forming a hydrophilic corona, and the hydrophobic blocks amass in the center of the nanostructures, forming a hydrophobic core, as a result of hydrophobic interactions in water.[38] Polymers capable of crystallization-driven self-

assembly first assemble as a result of such hydrophobic interactions, but, upon increasing the temperature of the suspension above the glass transition (T_g) and below the melting temperature of the hydrophobic block, the core block can rearrange and crystallize. CDSA further enables the generation of diverse nanostructure morphologies, in addition to morphologies that can be achieved using the typical hydrophobic interactions.[10]

The first defined 1D "living" CDSA nanostructures were reported by Manners and Winnik in the early 2000s for polymers with the crystalline hydrophobic core block, poly(ferrocenyldimethylsilane) (PFS).[42] Crystal growth is kinetically-controlled, and the growth from small monodisperse "seed" crystals can be controlled and reproduced when using the same assembly procedures because the length of the assembled morphologies increase predictably with time. A crystalline core enables self-assembly of polymers in solution to form nanostructures with low interfacial curvature, including 2D platelets and 1D fibers of high aspect ratios, providing an alternative to the packing parameter-controlled thermodynamic nanostructures. Such an alternative is beneficial because this allows access to more nanostructures than achievable by varying the composition of block copolymers. Significantly, in a "living" CDSA system, the ends of the crystals remain active, from which slow addition of free polymer (called unimer) will then extend the crystals. These seeds are formed by breaking crystals by sonication and can be used to initiate crystal growth upon addition of unimers. The use of such crystalline seeds results in nearly monodisperse cylindrical nanostructures, of which the length can be controlled from *ca.* 20 nm to 2 μm by modulation of the unimer to seed ratio.[43] Since then, nanostructures obtained by "living" CDSA includes core blocks comprised of polyethylene,[44-45] π-conjugated polymers,[46-47] and planar, π-stacking molecules,[48-52] among others.[43, 53-55] Morphologies resulting from "living" CDSA include a wide variety of micellar

architectures: segmented coronas including multi-block co-micelles such as monochrome and multi-color fluorescent "barcodes",[54-57] multi-armed micelles,[58] and non-centrosymmetric structures.[59]

More recently, CDSA of fully-organic polymers has been under investigation. CDSA of block copolymers comprised of a semi-crystalline, degradable PLLA segment has been studied by the Dove and O'Reilly groups. The aqueous coronas include poly(*N*,*N*-dimethylacrylamide), poly(ethylene glycol), and poly(4-acryloyl morpholine), and polyacrylic acid (PAA).[11] Of note, our group has developed a fully-degradable PLLA-based diblock polymer that undergoes CDSA.[12] Each system requires optimization of the solvent system and assembly conditions. The resulting morphologies appear to depend on the interplay between the glass transition of the PLLA core, the solubility of the corona block, and the rigidity of the hydrophilic block. There is an opportunity for exploration of CDSA of fully-degradable PLLA-based diblock polymers where the hydrophilic corona is of very low rigidity, as indicated by a glass transition below room temperature, such as the polymers in this thesis.

OUTLINE AND SCOPE OF THESIS

The morphology of PLLA-*b*-PC crystalline-core nanostructures was tuned by changing the composition of a fully degradable semi-crystalline polymer using CDSA. These polymers were modified using click chemistry to render them amphiphilic and assembled into nanostructures with diverse nanostructures using crystallization-driven self-assembly (CDSA).

The overall objective of this thesis is to generate a reliable methodology to access self-assembled fully-degradable nanostructures of controllable sizes and morphologies using CDSA conditions. To do this, first, a series of nine PLLA-*b*-PC-cys polymers was generated, consisting of a hydrophobic semi-crystalline PLLA block and a cysteine-functionalized hydrophilic polycarbonate block (PC-cys). The latter was synthesized by photo-initiated thiol-yne "click" reaction of cysteine onto the alkyne groups of the polycarbonate following ring-opening polymerization to render the block polymer amphiphilic prior to assembly. The molar mass and composition of each block were varied to generate an array of morphologies.

To induce CDSA, the solution of polymer was heated above the glass transition temperature of PLLA, *ca.* 55-60 °C.[10] The expectation was that PLLA-*b*-PC will be capable of generating cylindrical micelles using CDSA conditions that are not accessible using typical hydrophobic interactions – therefore, a fully-degradable system with an aliphatic hydrophilic corona that is more flexible than that of more rigid glucose-based analogues[12] will be characterized.

Following crystallization-driven self-assembly in water, AFM images showed spherical, cylindrical, and platelet-like morphologies depending on the ratio of the hydrophobic block to the hydrophilic block. Polymers with hydrophobic weight percentages <30% formed only spheres, whereas intermediate hydrophobic percentages (34% and 36%) produced platelets with

lengths of *ca.* 500 nm. Finally, the polymers with the highest weight percent (42% and 71%) yielded in large bundles of cylinders, *ca.* 500 nm or longer.

MATERIALS AND METHODS

Materials

1,5,7-triazabicyclo[4.4.0]dec-5-ene (TBD) (Sigma-Aldrich, 98%) was used as received and stored in inert atmosphere. 4-methylbenzyl alcohol (Aldrich, 98%) and *(S,S)*-3,6-Dimethyl-1,4-dioxane-2,5-dione (L-lactide) (Alfa Aesar, ≥98%) were recrystallized in ethyl acetate, dried over P_2O_5 *in vacuo* for 3 d, and stored under inert atmosphere. Acetic acid (glacial, Fisher Scientific) and hydrochloric acid (concentrated, Macron Inc.) was used as received. Tetrahydrofuran (THF), *N,N*-dimethylformamide (DMF), and dichloromethane (DCM) were purified by passage through a solvent purification system (JC Meyer Solvent Systems) before use. Dialysis membrane tubing with a molecular weight cut-off (MWCO) of 12-14 kDa was purchased from Spectrum Laboratories, Inc. and immersed for 5 min in nanopure water at room temperature before use.

Characterization

Column chromatography was performed using a CombiFlash Rf4x system (Teledyne ISCO).

^{1}H NMR and ^{13}C NMR spectra were recorded on either a Varian 300 or a Varian 500 spectrometer using VnmrJ software suite. Chemical shifts were referenced to solvent signals.

Fourier transform infrared (FTIR) spectra were recorded on an IR Prestige 21 system equipped with a diamond attenuated total reflection (ATR) lens (Shimadzu Corp., Japan) and analyzed using IRsolution *v.* 1.40 software.

Molar mass and molar mass distribution were determined by size exclusion chromatography (SEC) was conducted on a system equipped with Waters Chromatography, Inc. (Milford, MA) model 1515 isocratic pump and a model 2414 differential refractometer with a three-column set of Polymer Laboratories, Inc. Styragel columns (PLgel 5 μm Mixed C, 500 Å, and 104 Å, 300 ×

7.5 mm columns) and a guard column (PLgel 5 μm, 50 × 7.5 mm). The system was equilibrated at 40 °C in THF, which served as the polymer solvent and eluent (flow rate set to 1.00 mL/min). The differential refractometer was calibrated with Polymer Laboratories, Inc., polystyrene standards (300-467,000 Da). Polymer solutions were prepared at a concentration of *ca.* 3 mg/mL with 1% v/v toluene as a flow rate marker. Data were analyzed using Empower Pro software from Waters Chromatography, Inc.

Thermogravimetric analysis (TGA) was performed under N_2 atmosphere using a Mettler-Toledo TGA/SDTA851e with a heating rate of 10 °C/min from 25-500 °C. Glass transition (T_g) temperatures were measured by differential scanning calorimetry (DSC) on a Mettler-Toledo DSC822® calorimeter with a heating and cooling rate of 10 °C/min. Three heating and cooling cycles were conducted per trial. Data were analyzed using Mettler-Toledo Stare *v.* 7.01 software. The T_g was taken as the midpoint of the inflection tangent during the third heating scan.

Atomic force microscopy (AFM) was performed on a Multimode 8 system (Bruker, Santa Barbara, CA) in PeakForce® Tapping mode with ScanAsyst® image optimization software and a ScanAsyst-Air probe (k = 0.4 N/m, Bruker). Nanoparticle solutions (20 μL, 0.05 mg/mL) were deposited twice onto freshly-cleaved mica using a spin-coater programmed as follows: 1) 10 s, 500 rpm, 200 rpm/s; 2) 30 s, 3000 rpm, 200 rpm/s. If too few nanostructures were observed by AFM, the suspension was spin-coated twice more to increase the density of micelles on the mica. Average nanostructure heights were determined by the analysis of the AFM height images.

Methods

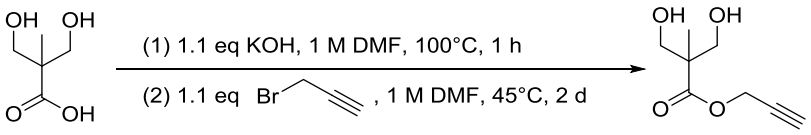

Figure 1. Synthesis of prop-2-yn-1-yl 3-hydroxy-2-(hydroxymethyl)-2-methylpropanoate

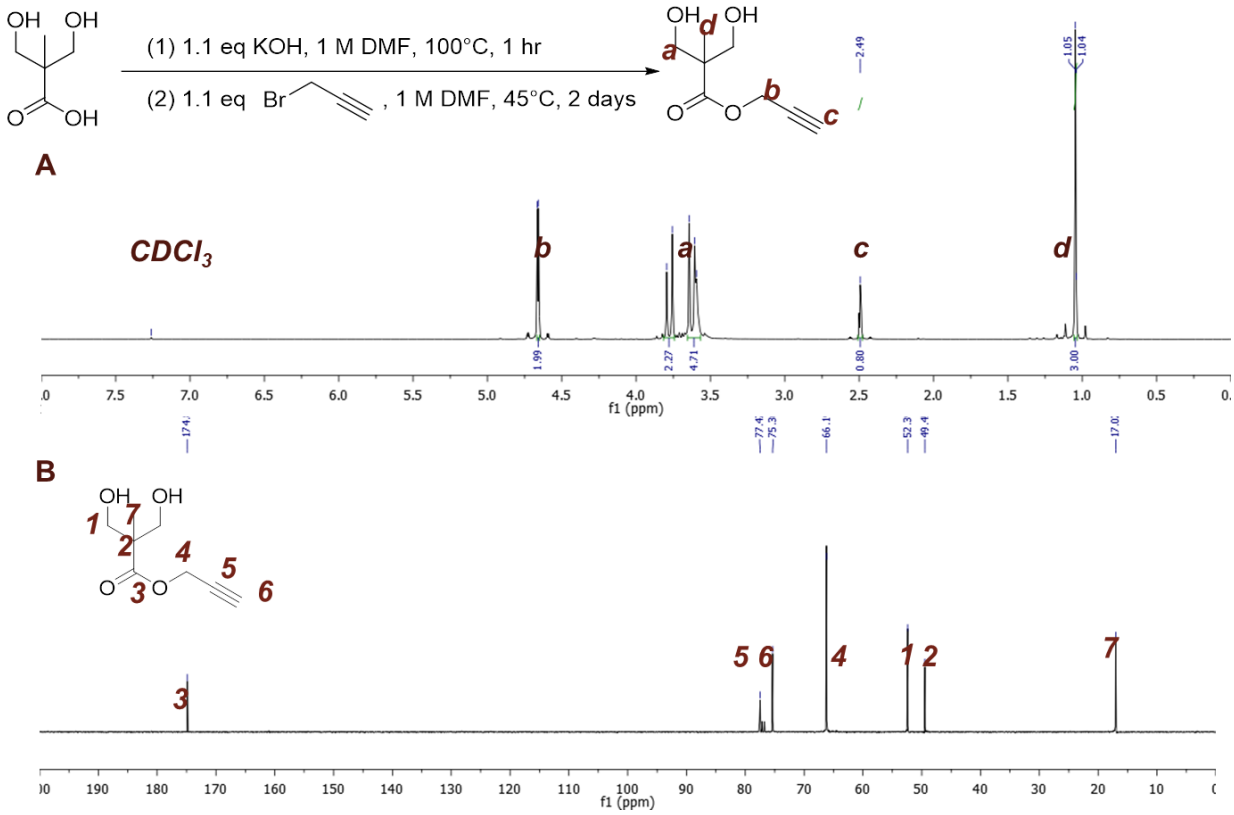

Figure 2. (**A**) ^{1}H NMR and (**B**) ^{13}C NMR spectra for the synthesis of prop-2-yn-1-yl 3-hydroxy-2-(hydroxymethyl)-2-methylpropanoate.

Synthesis of prop-2-yn-1-yl 3-hydroxy-2-(hydroxymethyl)-2-methylpropanoate

In a 100-mL round-bottom flask, a mixture of 3-hydroxy-2-(hydroxymethyl)-2-methylpropanoic acid (10 g, 74.6 mmol), potassium hydroxide (6.15 g, 74.6 mmol), and anhydrous DMF (57.3 mL, 0.5 M) was heated to 100 °C with stirring *via* magnetic stir bar for 1

h. The resulting colorless solution was cooled to 40 °C. Then, propargyl bromide (7.06 mL, 74.6 mmol) was added dropwise to the warm solution immediately resulting in the formation of a white precipitate. The reaction was allowed to proceed for 48 h at 40 °C until starting material was no longer observed by thin layer chromatography (TLC) (50% EtOAc/hex, R_f = 0.267, visualized using $KMnO_4$ solution). The mixture was then cooled to room temperature and the solvent was removed under reduced pressure. This residue was suspended in DCM and filtered to remove KBr salt. The filtrate was removed under reduced pressure and the product was isolated by column chromatography (50% EtOAc/hexanes). Product was dried *in vacuo* at room temperature. Yield (123.8 mg, 52%). (**Figure 1**) ^{1}H NMR (300 MHz, $CDCl_3$, ppm) δ = 4.80 (m, 2 H, C*H*$_2$CCH), 3.79-3.76 (d, *J* = 9.0 Hz, 2 H, *CH*$_2$OH), 3.64-3.61 (d, *J* = 9.0 Hz, 2 H, *CH*$_2$OH), 3.59 (m, O*H*), 2.49 (1 H, m, CC*H*), 1.05 (3 H, s, C*H*$_3$) ppm. ^{13}C NMR (300 MHz, $CDCl_3$) δ = 174.8, 77.5, 75.4, 662, 52.4, 49.45, 17.02 ppm. (**Figure 2**) FTIR: 1043, 1090, 1126, 1184, 1209, 1360, 1383, 1454, 1755 cm^{-1}.

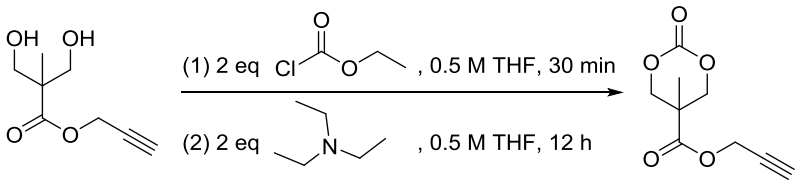

Figure 3. Synthesis of prop-2-yn-1-yl 5-methyl-2-oxo-1,3-dioxane-5-carboxylate

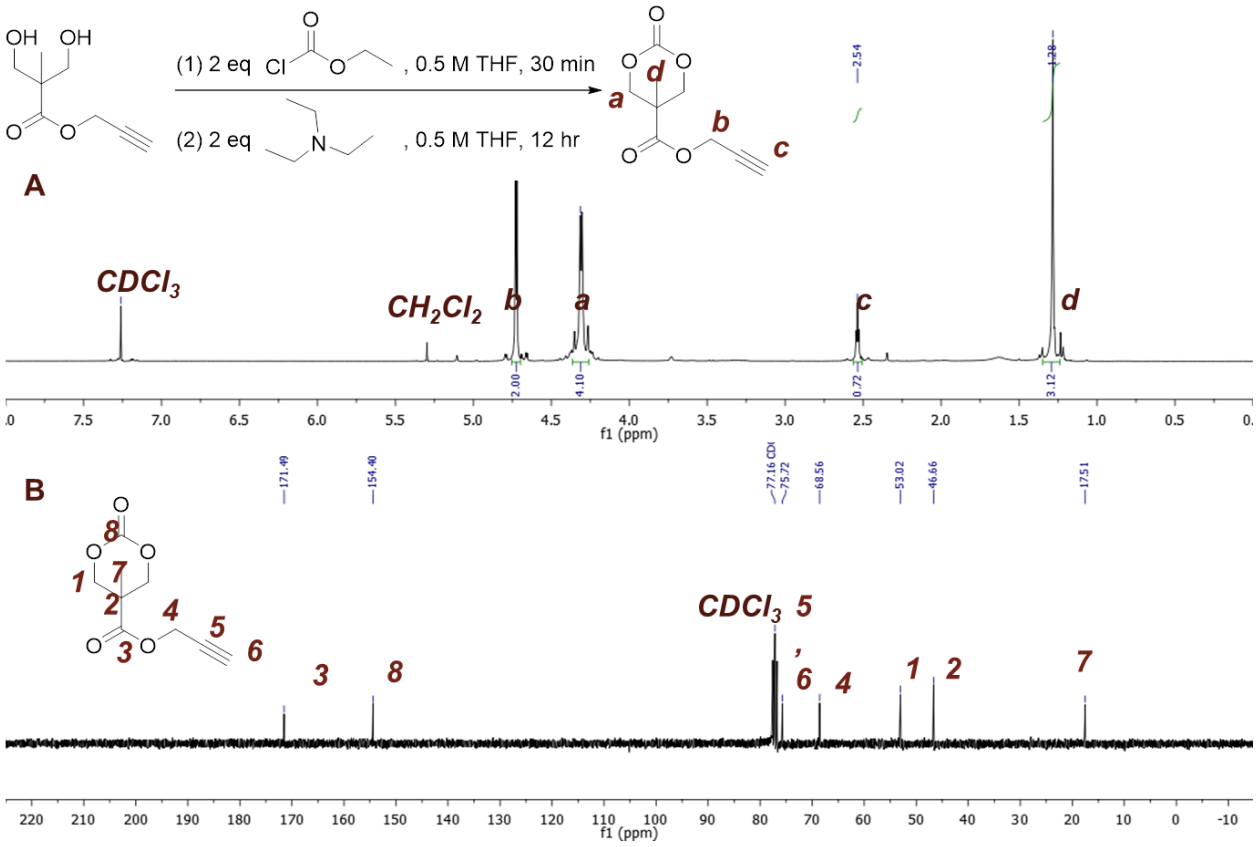

Figure 4. (**A**) ^{1}H NMR and (**B**) ^{13}C NMR spectra for the synthesis of prop-2-yn-1-yl 5-methyl-2-oxo-1,3-dioxane-5-carboxylate

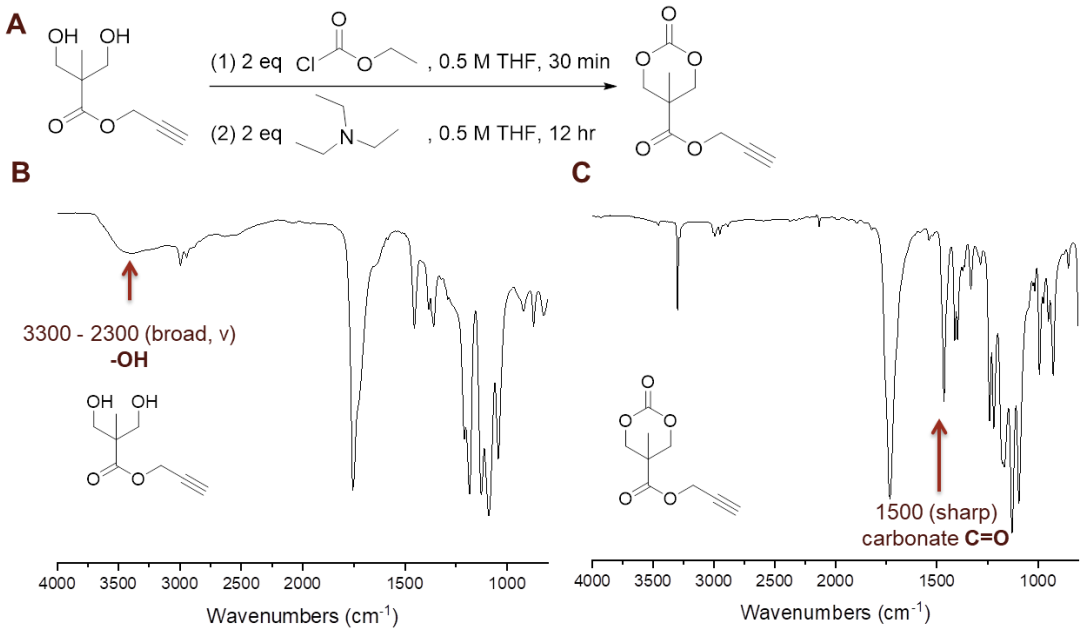

Figure 5. FTIR spectra for the synthesis of prop-2-yn-1-yl 5-methyl-2-oxo-1,3-dioxane-5-carboxylate: (**A**) reaction scheme; FTIR spectra of (**B**) prop-2-yn-1-yl 3-hydroxy-2-(hydroxymethyl)-2-methylpropanoate and (**C**) prop-2-yn-1-yl 5-methyl-2-oxo-1,3-dioxane-5-carboxylate

Synthesis of prop-2-yn-1-yl 5-methyl-2-oxo-1,3-dioxane-5-carboxylate

In a 100-mL round-bottom flask equipped with a stir bar, a colorless solution of prop-2-yn-1-yl 3-hydroxy-2-(hydroxymethyl)-2-methylpropanoate (5.189 g, 30.14 mmol) and dry THF (60.3 mL, 30.1 mmol) was cooled to 0 °C in an ice bath. Ethyl chloroformate (2.869 mL, 30.14 mmol) was added dropwise to the solution, which was then stirred at 0 °C for 2 h. After the starting material was no longer observed by TLC (50% EtOAc/hex), anhydrous triethylamine (4.2008 mL, 30.14 mmol) was added dropwise, resulting in a white suspension. This mixture was allowed to stir overnight at room temperature. Next, the solvent was removed under vacuum. The residue was suspended in acetone, filtered, evaporated to dryness, and then suspended in a small amount of 50% EtOAc/hexanes. The product was isolated by column chromatography

(0% to 40% EtOAc/hexanes). The prop-2-yn-1-yl 5-methyl-2-oxo-1,3-dioxane-5-carboxylate was recrystallized twice from EtOAc upon cooling, dried over P_2O_5 for 72 h, and then stored in under inert atmosphere prior to use in polymerizations. Yield (1.2 g, 20%). (**Figure 3**) ^{1}H NMR (300 MHz, $CDCl_3$) δ = 7.36 (m, 5 H, C*H*), 5.22 (s, 2 H, CH_2), 3.94 (q, 2 H, CH_2), 3.74 (q, 2H, CH_2), 2.77 (m, O*H*), 1.57 (m, O*H*), 1.08 (s, 3 H, CH_3) ppm. ^{13}C NMR (300 MHz, $CDCl_3$) δ =171.49, 154.40, 77.16, 75.72, 68.56, 53.02, 46.66, 17.51 ppm. (**Figure 4**) FTIR: 926, 949, 993, 1096, 1128, 1167, 1219, 1240, 1396, 1412, 1464, 1732, 3298 cm^{-1}. (**Figure 5**)

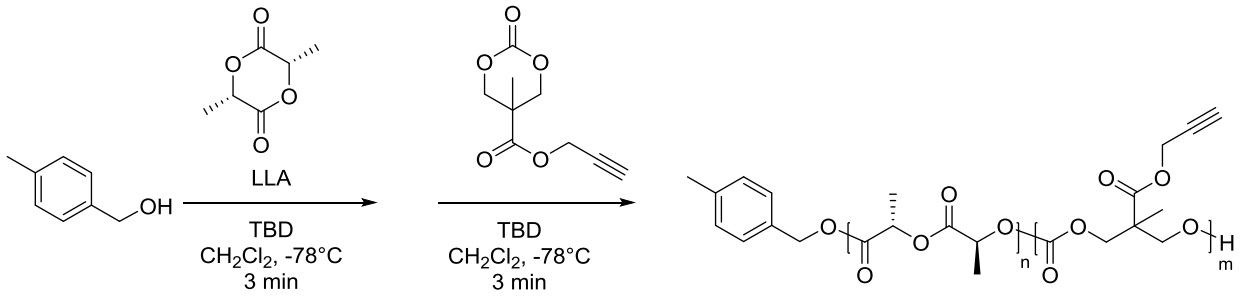

Figure 6. One-pot sequential ring-opening polymerization of L-lactide and prop-2-yn-1-yl 5-methyl-2-oxo-1,3-dioxane-5-carboxylate to yield the diblock PLLA-*b*-PC-alkyne

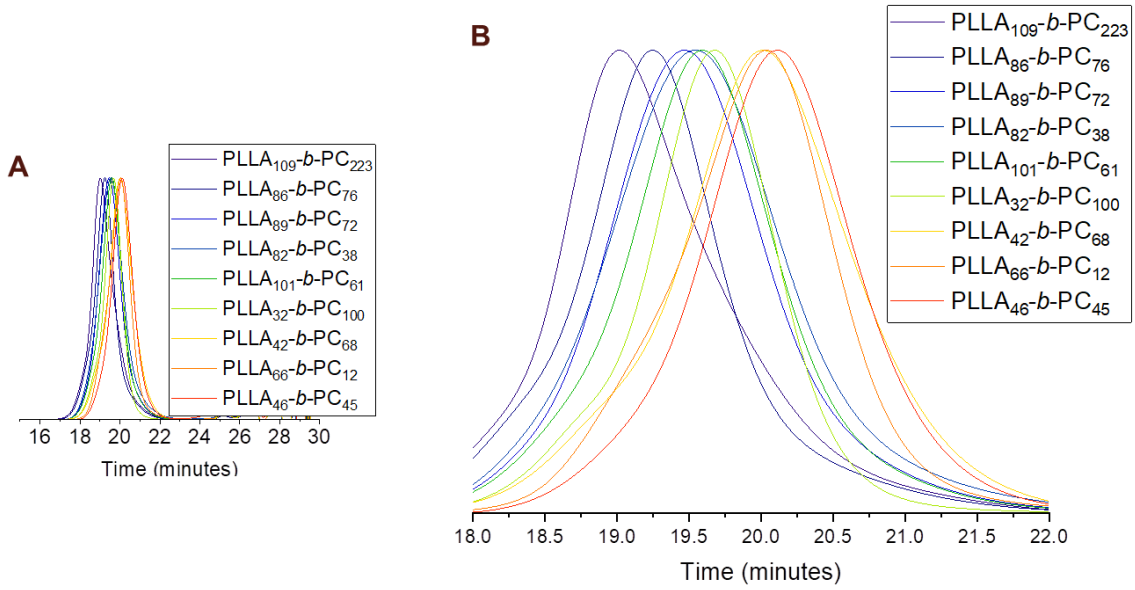

Figure 7. (**A**) SEC traces of PLLA-*b*-PC-alkyne; (**B**) enlarged

One-pot sequential polymerization to yield diblock PLLA-b-PC-alkyne

Under inert atmosphere in a glove box, 4-methyl benzyl alcohol (1 equiv., 4.1 mg, 0.003364 mmol), L-lactide (30 equiv., 145.4 mg, 1.009 mmol), and anhydrous DCM (2.02 mL, 0.5 M to monomer) were combined. While stirring in a -78 °C bath, the catalyst (TBD, 0.02 equiv., 2.81 mg, 0.02010 mmol) was added. After 3 min, the prop-2-yn-1-yl 5-methyl-2-oxo-1,3-dioxane-5-carboxylate (30 equiv., 200 mg, 1.009 mmol) was added. After 3 min, the reaction was quenched by addition of a small amount of glacial acetic acid. The polymer was purified by dropwise precipitation into *ca.* 100 mL of diethyl ether, and centrifugation at 10,000 rpm for 5 min at 5 °C three times. This polymer was evaporated to dryness under vacuum overnight and isolated as a white or colorless residue. ^{1}H NMR (500 MHz, DMSO-d_6) δ 7.21-7.15 (m, 4 H, Ar), 5.30 (s, 2 H, OCH_2Ar), 2.18-5.14 (m, 2*n* H, OC*H*CH$_3$), 4.73 (m, 2*m* H, OCH_2CCH), 4.34-4.28 (m, 4*m* H, CC*H*), 3.58-3.45 (m, 1*m* H, CC*H*), 2.35 (s, 3 H, ArCH_3), 1.58-1.57 (m, 3*n* H, CHCH_3), 1.29 (s, 3*m* H, CH$_2$CCH_3) ppm. ^{13}C NMR (125 MHz, DMSO-*d6*) δ =171.50, 169.62, 154.17, 78.30, 78.21, 69.06, 53.17, 46.67, 40.32, 17.09, 16.90. (**Figure 6**) FTIR: 973, 1044, 1082, 1128, 1181, 1213, 1241, 13354, 1425, 1493, 1500, 1509, 1523, 1534, 1541, 1546, 1551, 1749, 2947, 3010 cm^{-1}. SEC traces show symmetric peaks of *Đ* <1.2, suggesting a relatively monodistributed molar mass and living polymerization. (**Figure 7**)

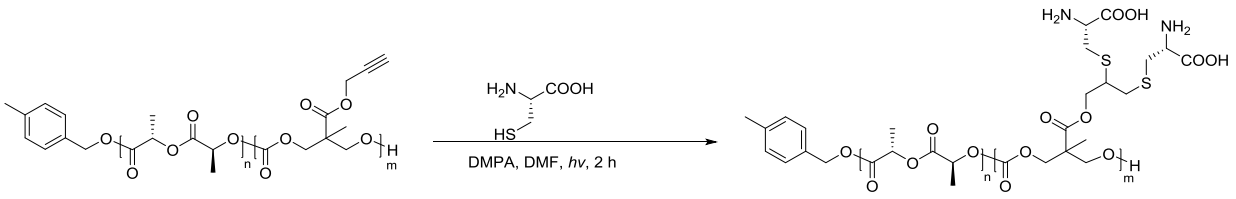

Figure 8. Post-polymerization functionalization of PLLA-*b*-PC -alkyne with cysteine *via* thiol-yne click reaction

Post-polymerization functionalization of PLLA-b-PC-alkyne with cysteine via thiol-yne click reaction

Alkyne-functionalized polymer (*e.g.*, 310 mg of $PLLA_{92}$-*b*-PC_{38}) was dissolved in anhydrous DMF (*ca.* 4 mL). Cysteine (1.2 g, 10 equivalents relative to alkyne moieties) was suspended in anhydrous DMF, and dissolved by addition of concentrated HCl and sonication, and then added to the polymer solution. The reaction mixture was deoxygenated for 5 min with $N_{2(g)}$. DMPA (7.6 mg, 0.03 equivalents to alkyne moieties), and the mixture irradiated at 365 nm for 2 h, and purified by dialysis in nanopure water (2 L batches containing 1-2 mL concentrated HCl), changing the solutions every 12 h for 3 d. Cysteine-functionalized polymer was isolated by lyophilization of the aqueous solution. (**Figure 8**) ^{1}H NMR (500 MHz, DMSO) δ 7.17-7.15 (m, 4 H, Ar), 5.14 (m, 2 + 2*n* H, OC*H*$_2$Ar, OC*H*CH$_3$), 4.25-4.15 (m, 2*m* + 2*m* H, O*CH*$_2$, O*CH*$_2$), 3.28-2.81 (m, 3*m* + 4*m* + 2*m* H, OC*H*$_2$*CH*, S*CH*$_2$, S*CH*$_2$CH), 2.25 (s, 3 H, ArC*H*$_3$), 1.42 (s, 6*n* H, C*H*$_3$), 1.16 (s, 3 H, C*H*$_3$) ppm. FTIR: 419, 442, 598, 650, 687, 770, 802, 926, 949, 993, 1095, 1128, 1167, 1219, 1240, 1396, 1412, 1464, 1732, 3298 cm^{-1}.

CDSA of PLLA-b-PC-cys to assemble nanoparticles in water

To assemble the nanoparticles, the polymer was suspended in nanopure water at 0.05 mg/mL. This suspension was heated at 65 °C for 30 h, and then cooled to room temperature.

RESULTS AND DISCUSSION

Synthesis and characterization of PLLA-*b*-PC-cys

Block copolymers of L-lactide and alkyne-functionalized cyclic carbonate (PLLA-*b*-PC-alkyne) were synthesized with varying block lengths and ratios. NMR spectroscopy was used to determine block ratios and lengths, while SEC was used to determine the molar mass distributions. The alkyne groups were modified with cysteine by photo-initiated thiol-yne click chemistry to afford the amphiphilic block polymer PLLA-*b*-PC-cys. NMR and IR spectroscopies were used to characterize the modification reaction, by comparing the spectra of the alkyne- and cysteine-modified block polymers. Thermal properties were evaluated before and after cysteine modification by TGA and DSC. CDSA of the cysteine-modified polymer yielded spheres, platelets, and cylindrical bundles, depending on the block length and ratio, as determined by AFM.

For the goal of creating cylindrical or other varied morphologies, PLLA was chosen as the hydrophobic block to enable crystallinity-driven self-assembly. A six-membered cyclic carbonate with a pendent alkyne was selected for the ROP of the hydrophilic block due to the relative ease of post-polymerization functionalization of the monomer. While ROP provides an efficient route to degradable polymers with narrow molar mass distributions and controlled architectures and composition, it is not tolerant of charged functional groups. To circumvent this, alkynes can be used to install hydrophilic groups after polymerization *via* a number of "click" reactions to render the polymer amphiphilic. Among these is the UV-catalyzed thiol-yne "click" reaction which can be used to incorporate a variety of molecules including cysteine, onto alkyne-functionalized polymers. Furthermore, L-lactide[60] and cysteine[61] are easily sourced biomolecules, and the synthesized block polymers PLLA-*b*-PC have ester and carbonate

linkages, rendering them hydrolytically degradable, and preventing long-term accumulation in the body.

In this work, varying the feed ratio of monomers resulted in hydrophobic to hydrophilic molar ratios of the generated polymers ranging from 1 : 2.2 to 6.3 : 1 as a ratio of repeating units, M_n 14.4 - 38.9 kDa, and PLLA weight percents from 13 to 71%. Block lengths were selected to correspond with literature previously published by our group on CDSA of analogous glucose-based PLLA-*b*-PCs of M_n 22-55 kDa and PLLA weight percents of 5 to 34% to yield morphologies ranging from spheres to cylinder bundles.[12] The carbonate in this work was hypothesized to yield an aliphatic corona, the increased flexibility of which would correspond with a lower overall T_g, compared to that of the more rigid PLLA-*b*-PGC with a higher T_g.[12] This added flexibility was hypothesized to also increase the PLLA weight percent that is needed to achieve cylinders, platelets, and bundles, as a lower T_g is associated with increased chain movement.

Sequential ring-opening polymerization (ROP) and post-polymerization thiol-yne click reaction were then used to generate a series of poly(L-lactide)-*b*-polycarbonates functionalized with cysteine (PLLA-*b*-PC-cys). The polymerization was carried out using TBD, which catalyzes ring-opening polymerizations of six-membered cyclic esters under metal-free conditions.[62] To a reaction vial containing L-lactide was added a small amount of TBD (0.02 equivalents), which facilitated quantitative monomer conversion in *ca.* 3 min, after which cyclic carbonate was added to form the second block, also converting quantitatively in *ca.* 3 min.[12] The reaction was quenched with a small amount of acetic acid and purified by precipitation into diethyl ether.

After polymerization, SEC data were collected of each sample to characterize the number-average molecular mass and molar mass distribution relative to polystyrene standards (**Table 1**). Dispersity ranged from $Đ$ = 1.07 to 1.17 – all under $Đ$ = 1.20, which is typically taken as an indication of living polymerization. Block lengths were also characterized by end group analysis of the proton NMR spectra (**Figure 8**). The integrations of the two protons of the α-carbon on the polylactide at *ca.* 5.25 ppm (2*n* H, where *n* is the number of PLLA repeat units – peak **e**), the four protons of the β-carbon on the polycarbonate backbone at *ca.* 4.15 ppm (4*m* H, where m is the number of polycarbonate repeat units – peak **g**) and the two protons on the propargyl ester functionality at *ca.* 4.75 ppm (2*m* H, where *m* is the number of polycarbonate repeat units – peak **i**) were compared against the methyl group on the 4-methyl benzyl end group at *ca.* 2.25 ppm (3 H – peak **a**) (**Figure 9**).

Post-polymerization modification of the alkyne-functionalized PLLA-*b*-PCs was conducted under irradiation at 365 nm. First, cysteine was added to DMF and concentrated HCl was added dropwise until the cysteine was protonated, increasing its solubility in DMF. The solution was then added to the polymer, and the resulting mixture was deoxygenated by sparging with nitrogen, and a small amount of DMPA was added prior to UV irradiation for 2 h. A large excess of cysteine was used (10:1 molar equivalents of cysteine to alkyne) to drive the reaction towards completion. Proton NMR spectroscopy showed upfield shifts of the two protons adjacent to the propargyl group (peak **i**) and the four protons of the β-carbon of the polycarbonate backbone (peak **g**) upon substitution with cysteine. Additionally, the disappearance of the terminal alkyne proton (peak **j**), and the appearance of three new proton resonances corresponding to cysteine (peaks **m, k, l**) suggested successful conversion of the alkynes (**Figure 9**). In the ^{13}C NMR spectrum, the disappearance of the alkyne signal at *ca.* 78

ppm after the click reaction was performed further supports the complete conversion of the alkyne (**Figure 10**). Unfortunately, the low solubility of the cysteine-functionalized polymers results in a low signal-to-noise ratio in the ^{13}C NMR spectrum that prevents further conclusions about the cysteine functionalization, particularly a new carbonyl signal *ca.*170 ppm. IR spectroscopy also indicates that conversion occurred, as a new carbonyl stretch signal appears at *ca.* 1600 cm^{-1}, corresponding to the cysteine carboxylic acid, and broad stretches also appeared at *ca.* 2300-3300 cm^{-1}, corresponding to the cysteine carboxylic acid and amine (**Figure 11**).

Table 1. Summary of the degree of polymerization, molar mass, dispersity, and percent weight of hydrophobic block, as it corresponds to the resulting morphology of overnight CDSA at 0.05 mg/mL in water.

	$M_{n\ NMR}$[a] (kDa)	$M_{n\ SEC}$[b] (kDa)	$Đ$	n:m[a]	PLLA wt% (after cysteine functionalization)	Observed morphology
$PLLA_{109}$-*b*-PC_{223}-cys	38.9	60.0	1.17	1 : 2.2	18	spheres
$PLLA_{42}$-*b*-PC_{68}-cys	23.8	19.6	1.17	1 : 1.6	22	spheres
$PLLA_{32}$-*b*-PC_{100}-cys	19.4	24.6	1.10	1 : 1.5	13%	spheres
$PLLA_{46}$-*b*-PC_{45}-cys	14.4	15.7	1.13	1 : 1	32%	spheres
$PLLA_{86}$-*b*-PC_{76}-cys	36.8	27.6	1.17	1.1 : 1	34%	platelets
$PLLA_{89}$-*b*-PC_{72}-cys	31.1	27.1	1.16	1.2 : 1	36%	platelets
$PLLA_{101}$-*b*-PC_{61}-cys	19.2	26.7	1.07	1.7 : 1	43%	bundles
$PLLA_{82}$-*b*-PC_{38}-cys	30.5	19.5	1.17	2.1 : 1	49%	platelets
$PLLA_{66}$-*b*-PC_{12}-cys	16.1	11.9	1.12	6.3 : 1	71%	bundles

[a] Determined by ^1H NMR spectroscopy (500 MHz) in $CDCl_3$.
[b] Estimated relative to polystyrene standards by SEC eluting in THF.

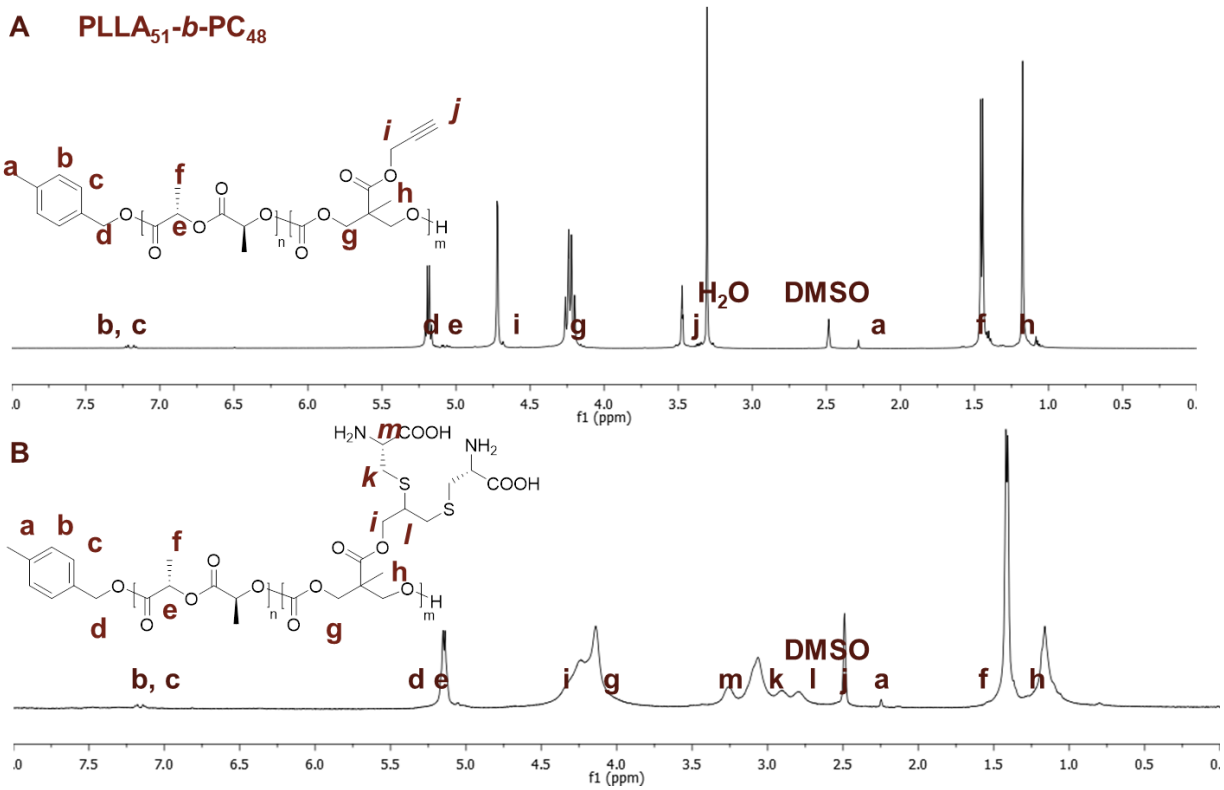

Figure 9. ^{1}H NMR spectra of (**A**) PLLA$_{51}$-*b*-PC-alkyne$_{48}$ and (**B**) PLLA$_{51}$-*b*-PC-cys$_{48}$ showing the conversion of the alkyne to append cysteine moieties

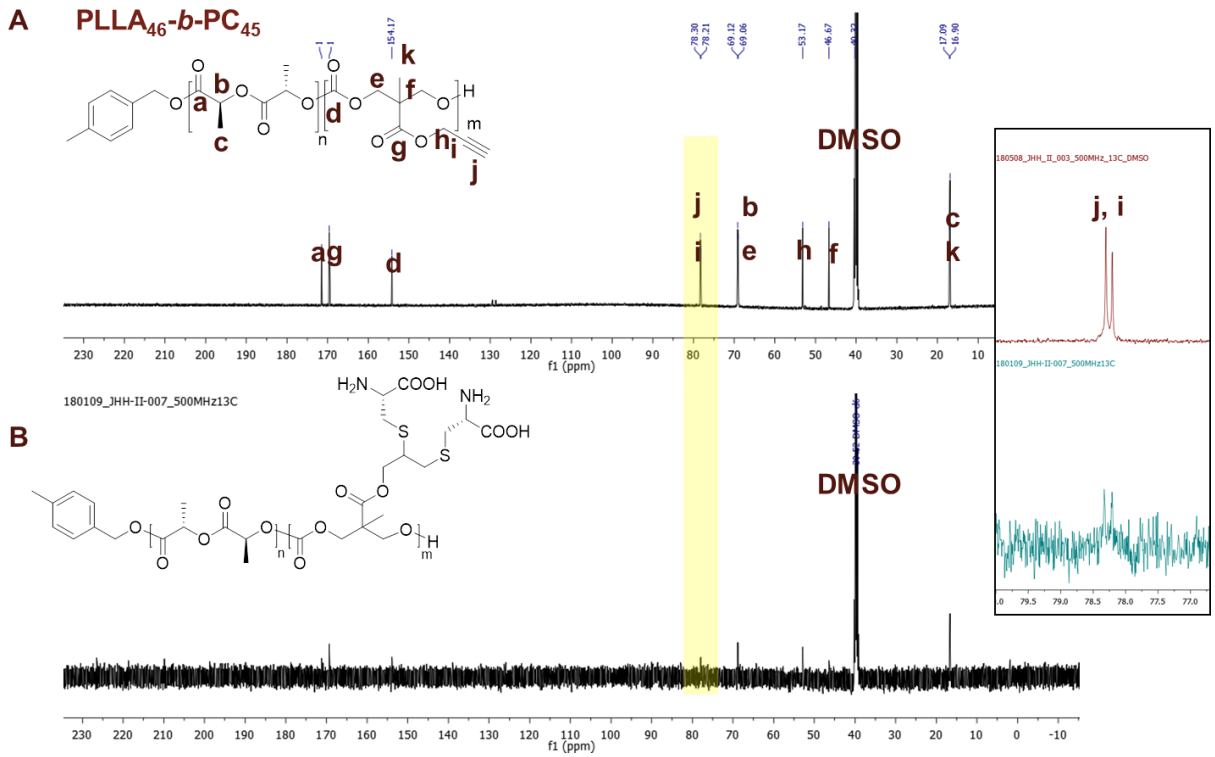

Figure 10. ^{13}C NMR spectra of (**A**) PLLA$_{46}$-*b*-PC-alkyne$_{45}$ and (**B**) PLLA$_{46}$-*b*-PC-cys$_{45}$ showing the conversion of the alkyne to append cysteine moieties

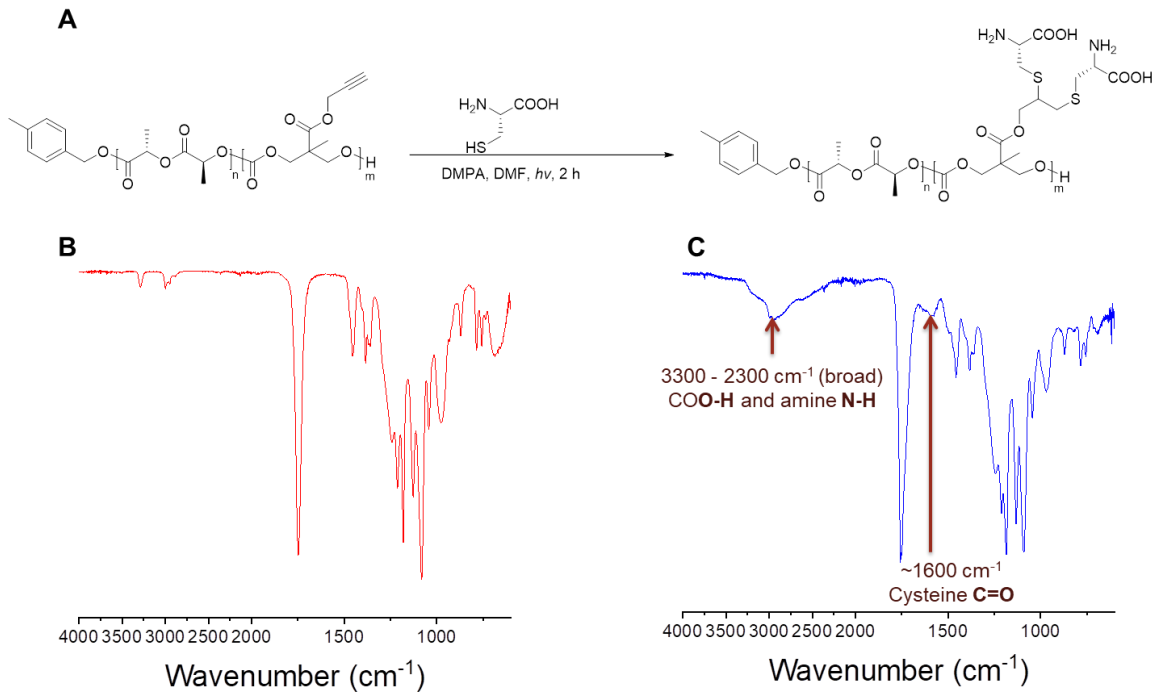

Figure 11. Conversion of the alkyne to cysteine moiety post-polymerization: reaction scheme (**A**), and the IR spectrum of the (**B**) PLLA$_{101}$-*b*-PC-alkyne$_{61}$ and (**B**) PLLA$_{101}$-*b*-PC-cys$_{61}$

Thermogravimetric analysis (TGA) of cysteine-functionalized PLLA-*b*-PC-cys showed a two-stage mass loss, from 150-225 °C, and from 250-300°C (**Figure 12** and **Table 2**). As the initial mass loss was not observed in the polymer prior to cysteine functionalization, this mass loss likely corresponds to decomposition of the cysteine units. The molar ratio of polycarbonate to polylactide molar repeat unit was determined by NMR of the alkyne-modified polymers given the insolubility of the cysteine-modified polymers, and the resulting calculated percent weight of cysteine, agrees with the value of weight loss between 150-225 °C. (**Figure 13**)

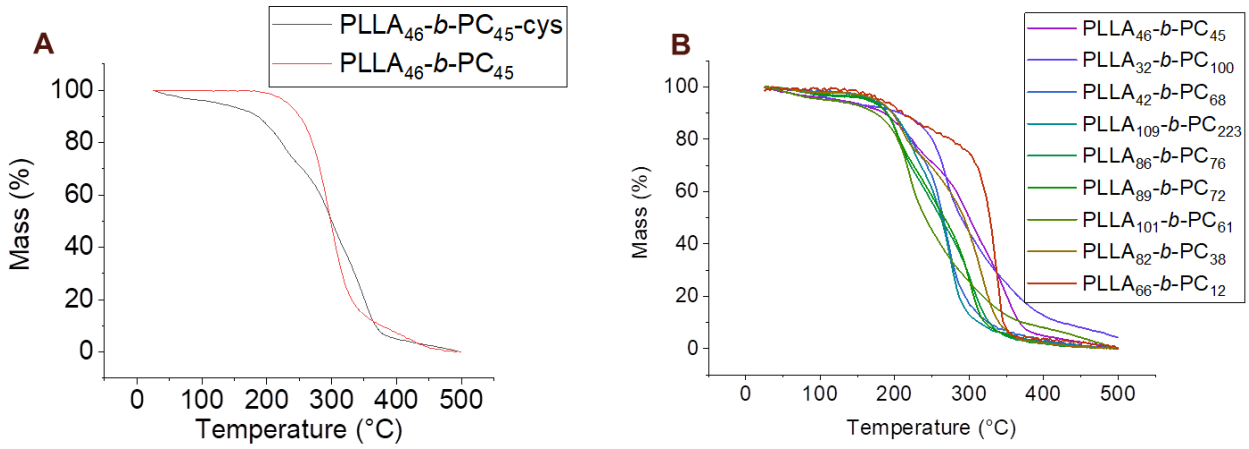

Figure 12. TGA thermograms of (**A**) $PLLA_{46}$-*b*-PC_{45} before and after cysteine modification, and (**B**) of different compositions of $PLLA_n$-*b*-PC-cys_m.

Table 2. Summary of degree of polymerization, molar mass, and percent weight of cysteine, as it corresponds to the resulting mass loss at various temperatures measured by TGA.

	% weight cysteine[a]	% mass loss from 25-100 °C	% mass loss from 150-225 °C	% mass remaining at 400 °C
$PLLA_{46}$-*b*-PC_{45}	12	0	14	15
$PLLA_{89}$-*b*-PC_{72}	24	2	22	8
$PLLA_{82}$-*b*-PC_{38}	27	4	29	5
$PLLA_{86}$-*b*-PC_{76}	32	2	28	9
$PLLA_{32}$-*b*-PC_{100}	33	3	29	11
$PLLA_{66}$-*b*-PC_{12}	34	4	21	5
$PLLA_{109}$-*b*-PC_{223}	42	1	20	12
$PLLA_{42}$-*b*-PC_{68}	45	2	22	14
$PLLA_{101}$-*b*-PC_{61}	49	5	53	9
[a] Determined by ^{1}H NMR spectroscopy (500 MHz) in $CDCl_3$.				

PLLA block copolymers were expected to exhibit a moderately high T_g, corresponding to that of the PLLA homopolymer (T_g 60-65 °C). However, DSC thermograms of PLLA-*b*-PC-alkyne revealed unusually low T_gs (20-32 °C) (**Figure 14**). This is likely due to the mixing of PLLA and PC components to form a homogeneous material. The glass transition behaviors of polymer blends are greatly influenced by the compatibility of their components. Copolymers that form homogeneous materials typically exhibit a single T_g, whereas two glass transitions are expected for copolymers that phase-segregate.[36] The Fox-Flory equation was used to predict the

T_g for each sample prior to the cysteine functionalization, using the T_g of PLLA (T_g 60-65 °C) and that of the alkyne-functionalized PC (*ca.* 9.3 °C), and the weight percentages of each block as determined by NMR spectroscopy (**Figure 15**). The predicted values agree with the observed T_g, correctly predicting an exponential decrease of T_g as the weight percent of the hydrophilic block increases and consistent with the homogeneous mixing of the two blocks. Interestingly, after the click reaction, no T_g was observed between 0 and 150 °C. This may be due to the incorporation of water into the polymer due to the more hygroscopic nature of the zwitterionic cysteine moieties, thereby plasticizing the sample.

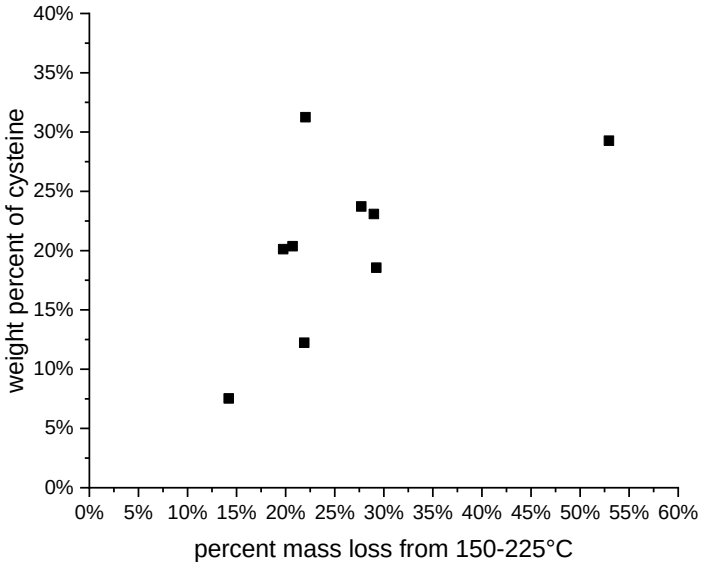

Figure 13. Percent mass loss at 150-225 °C, as determined by TGA, as a function of the percent weight of cysteine of PLLA-*b*-PC-cys. The percent mass loss between 150-225 °C increased with the ratio of polycarbonate to polylactide repeating units.

Table 3. Glass transitions of PLLA-*b*-PC-alkynes

	% wt hydrophilic before cysteine functionalization	$T_{g,\ cooling\ curve}$ (°C)	$T_{g,\ heating\ curve}$ (°C)	$T_{g,\ average}$ (°C)	$T_{g,\ predicted}$ (°C)
$PLLA_{109}$-*b*-PC_{223}	74	17	25	21	12
$PLLA_{42}$-*b*-PC_{68}	78	6	3	5	13
$PLLA_{32}$-*b*-PC_{100}	81	6	-3	2	11
$PLLA_{46}$-*b*-PC_{45}	57	23	17	20	15
$PLLA_{86}$-*b*-PC_{76}	55	22	21	22	15
$PLLA_{89}$-*b*-PC_{72}	52	14	9	12	16
$PLLA_{101}$-*b*-PC_{61}	45	5	-0	2	17
$PLLA_{82}$-*b*-PC_{38}	39	-4	--	-4	19
$PLLA_{66}$-*b*-PC_{12}	19	--	--	--	29

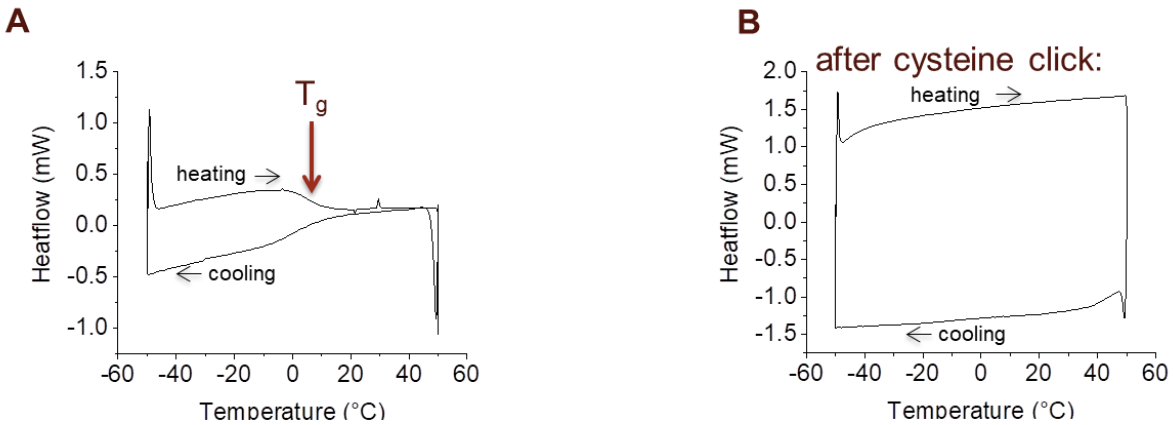

Figure 14. DSC thermograms show significantly lower total T_gs of PLLA-*b*-PC-alkynes (**A**) compared to PLLA (T_g of *ca.* 65 ºC). After the click reaction (**B**), no observed T_g was observed. The heating traces are on the bottom and the cooling traces on the top.

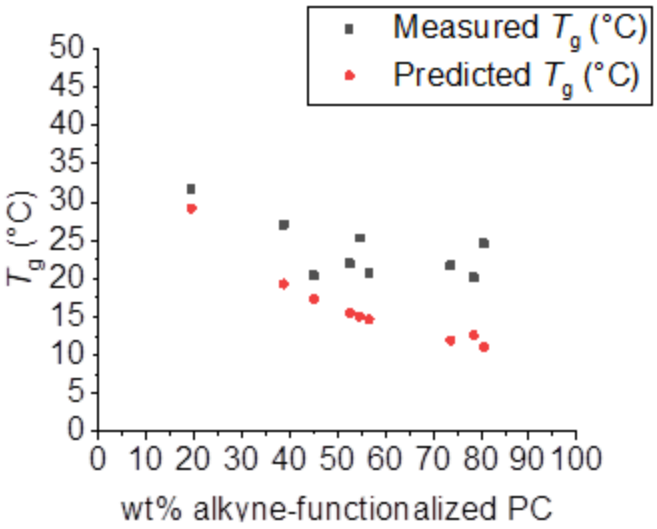

Figure 15. Measured and predicted T_g values listed as a function of weight percentage of the alkyne-functionalized polycarbonate block. Predicted values were calculated from the Fox-Flory equation. Measured values were collected by DSC with a heating and cooling rate of 10 °C/min. Three heating and cooling cycles were conducted per trial. The T_g was taken as the midpoint of the inflection tangent of the third heating scan.

Crystallization-driven self-assembly of PLLA-*b*-PC-cys

For CDSA, the polymer was suspended in nanopure water at 0.05 mg/mL and heated at 65 °C for 30 h, which is above the T_g of PLLA to enable enhanced chain motion and assembly, and then cooled to room temperature. The polymer concentration was selected to match the assembly conditions of a higher T_g glucose carbonate-based analogs so that the results of the assembly experiments could be compared.[12] The size and morphology of the resulting assemblies were characterized by AFM.

Following crystallization-driven self-assembly in water, AFM images showed spherical, cylindrical, or platelet-like morphologies depending on the ratio of the hydrophobic block to the hydrophilic block.

Table 4. Summary of molar mass, percent weight of hydrophobic block, and height based on AFM images, as it corresponds to the resulting morphology of overnight CDSA at 0.05 mg/mL in water.

	$M_{n\ NMR}$[a] (kDa)	PLLA wt% (after cysteine functionalization)	Observed morphology	Height of assemblies[b]
$PLLA_{109}$-*b*-PC_{223}	38.9	18	spheres only	2 ± 1 nm
$PLLA_{42}$-*b*-PC_{68}	23.8	22	spheres only	1 ± 1 nm
$PLLA_{32}$-*b*-PC_{100}	19.4	13	spheres only	2 ± 1 nm
$PLLA_{46}$-*b*-PC_{45}	14.4	32	spheres only	9 ± 2 nm
$PLLA_{86}$-*b*-PC_{76}	36.8	34	platelets	16 ± 5 nm
$PLLA_{89}$-*b*-PC_{72}	31.1	36	platelets	10 ± 3 nm
$PLLA_{101}$-*b*-PC_{61}	19.2	43	bundles	10 ± 3 nm
$PLLA_{82}$-*b*-PC_{38}	30.5	49	platelets	14 ± 4 nm
$PLLA_{66}$-*b*-PC_{12}	16.1	71	bundles	10 ± 2 nm

[a] Determined by ^{1}H NMR spectroscopy (500 MHz) in $CDCl_3$.
[b] Estimated using AFM images

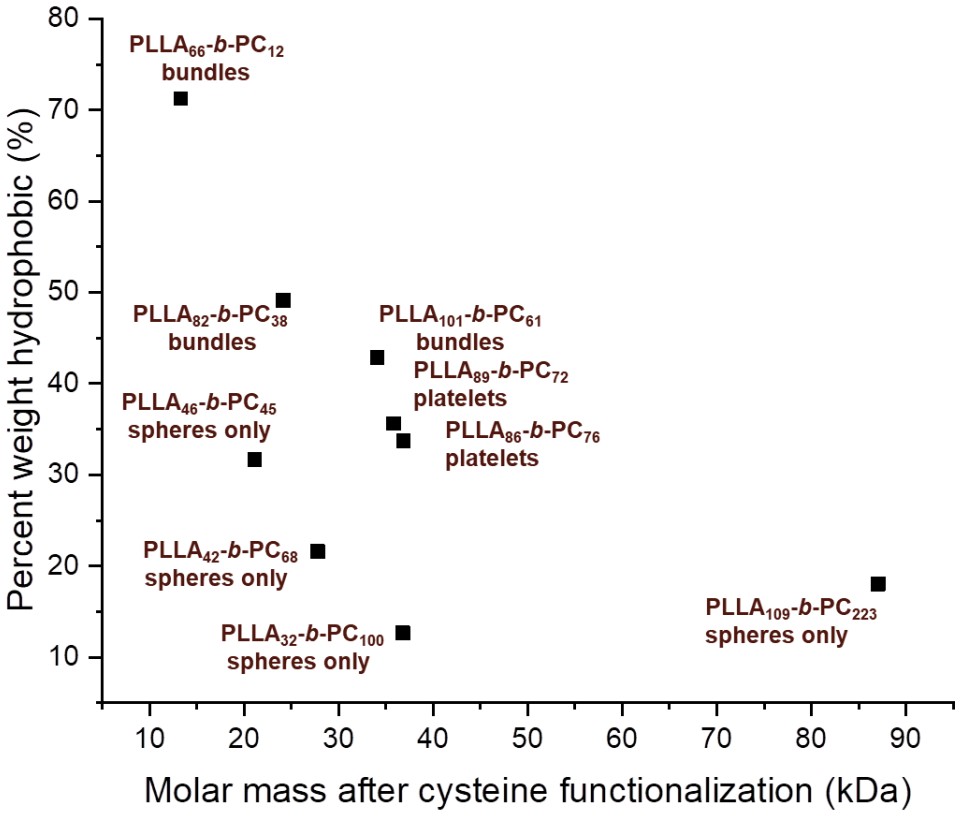

Figure 16. Observed morphologies of PLLA-*b*-PC-cys, as a function of total molar mass and hydrophobic weight percent.

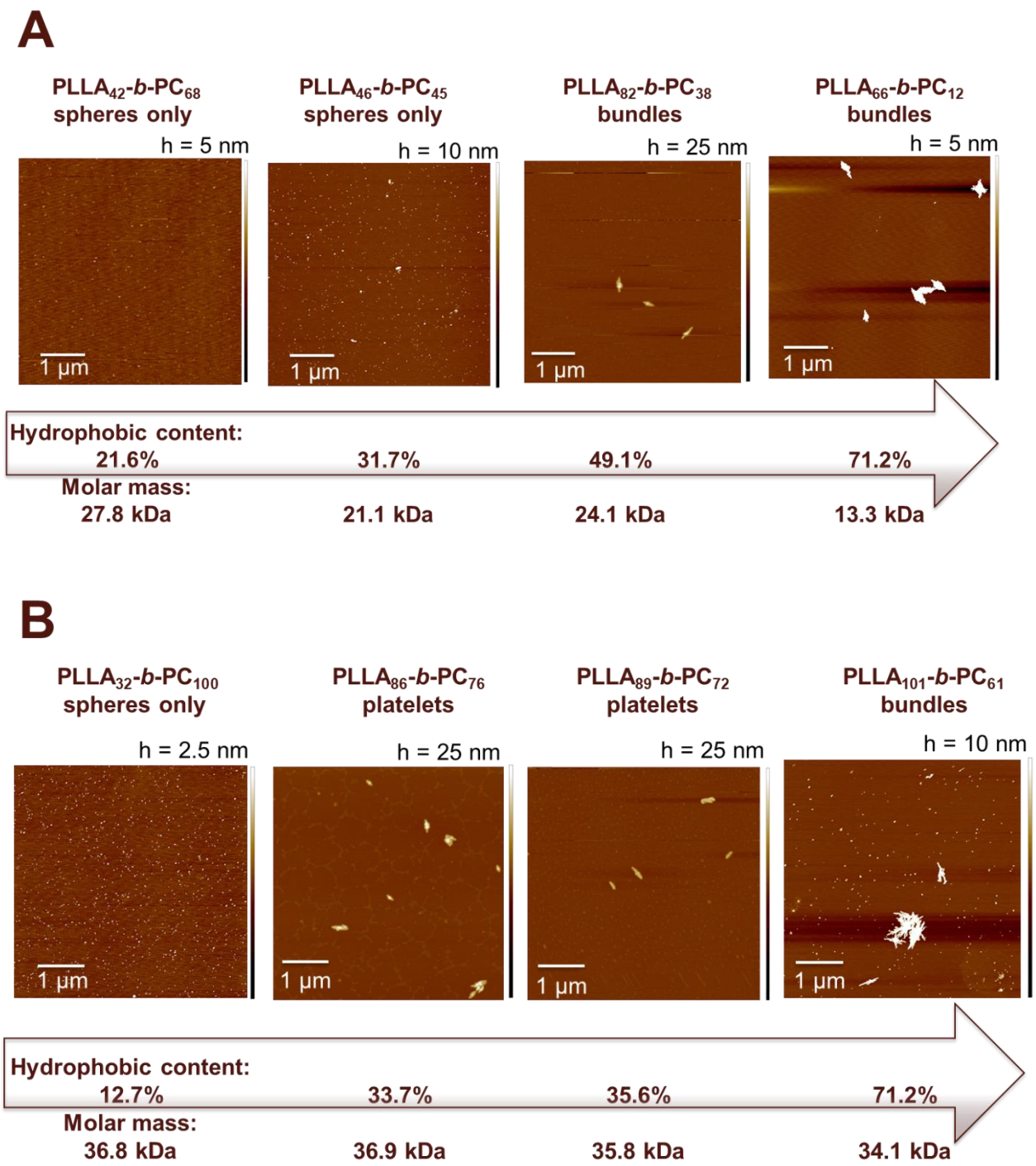

Figure 17. (A) Polymers of low molar mass (<30 kDa) begin to form bundles at hydrophobic content 49 wt% , while **(B)** those of intermediate molar mass (30-40 kDa) only need hydrophobic content of 34 wt% to begin forming platelets.

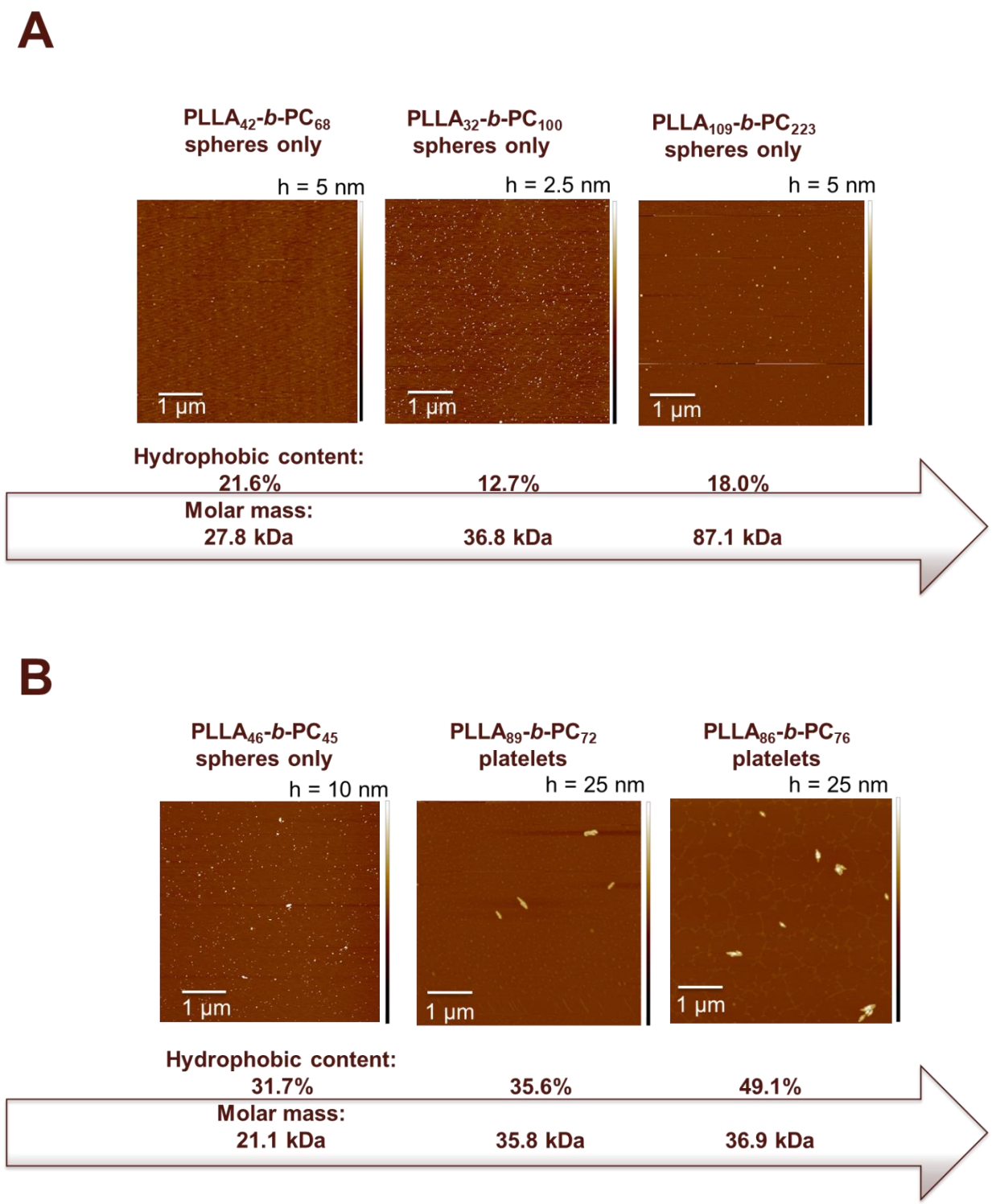

Figure 18. (A) Polymers of low wt% PLLA (<30 wt%) form spheres only, even up to 87 kDa, while **(B)** polymers with 30-40 wt% PLLA begin to form platelets at >36 kDa, and **(C)** polymers with 40-50 wt% PLLA form bundles even at 24 kDa.

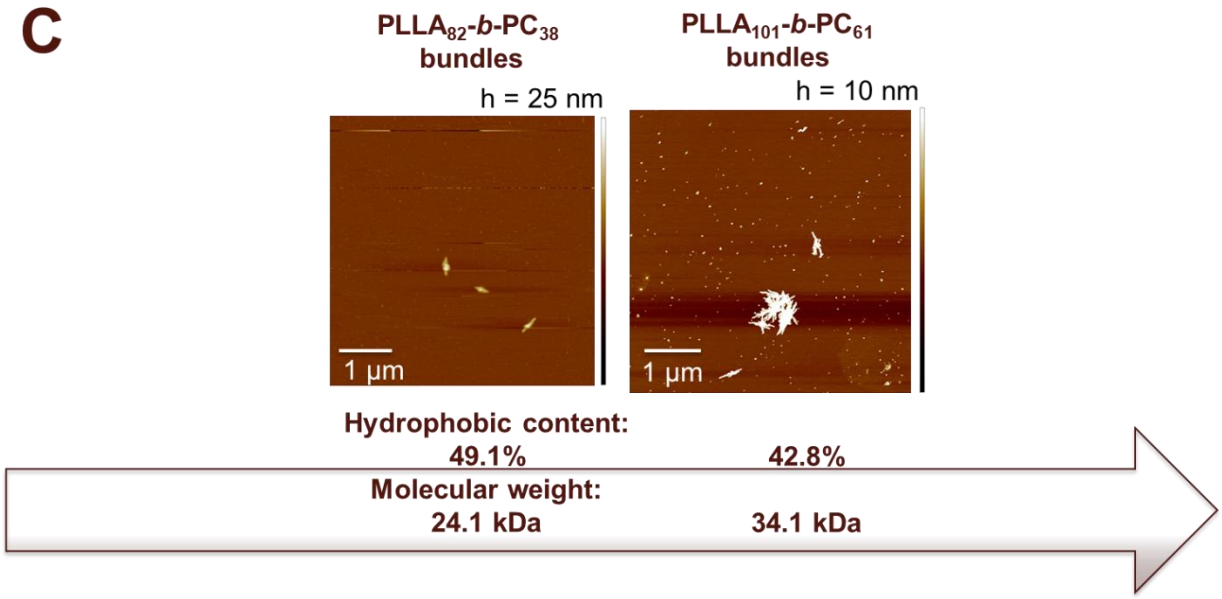

Figure 18 Continued.

Hydrophobic content and molecular weight was found to impact the morphology of the nanostructures obtained from CDSA of PLLA-*b*-PC-cys. Polymers of low molar mass (<30 kDa) formed bundles at hydrophobic contents of 49 wt%, while those of intermediate molar mass (30-40 kDa) formed platelets at lower hydrophobic content (34 wt%) (**Figure 17**). In terms of hydrophobic content, polymers with <30 wt% PLLA formed spheres only, even up to 87 kDa, whereas polymers of intermediate hydrophobic wt% (30-40 wt% PLLA) formed platelets at >36 kDa. Block polymers with 40-50 wt% PLLA formed bundles even at the relatively low molar mass of 24 kDa (**Figure 18**).

These findings are consistent with other work in the literature, where block polymers with lower hydrophobic components typically afford spherical micelles in water, while those with a higher hydrophobic weight percent allowed access to cylinders, platelets, lamellae, and other unusual morphologies. The previously-published analogous glucose-based structures with higher glass transitions and M_n of 30.1-55.4 kDa yielded spheres with <7 wt% of PLLA,

cylinders from block polymers with 13-19% weight of PLLA, and platelets at 34% wt of PLLA (**Figure 19**).[12] These findings suggest that T_g of the corona reflects its relative flexibility. A more flexible corona requires more weight percent PLLA in order to access CDSA-formed morphologies. Another report of CDSA of poly(acrylic acid)-*block*-poly(lactide) (PAA-*b*-PLLA) demonstrated that spheres were formed when the hydrophobic weight <15%; cylinders are formed where the hydrophobic weight percent was between 15% and 37%; and a mixture of cylindrical and lamellar particles for hydrophobic weight percent of 63.4%. [63]

These results indicate that, for all systems, the different morphologies observed as a function of molecular weight and hydrophobic weight percent as compared to those reported in the literature emphasize the need to conduct these studies for individual systems, as compositional variables can certainly be expected to dictate morphology. Gratifyingly, there is a general trend where rigidity of the polymer backbone (for example, the PLLA-*b*-PGC-cys) should be expected to have a higher T_g than the block polymers containing aliphatic polycarbonates (PLLA-*b*-PC-cys), despite the similar cysteine modification of both polymers. Further, as expected, the weight percent necessary to attain cylinders is lower in the more rigid poly(glucose carbonate) system than in the more flexible aliphatic polycarbonate.

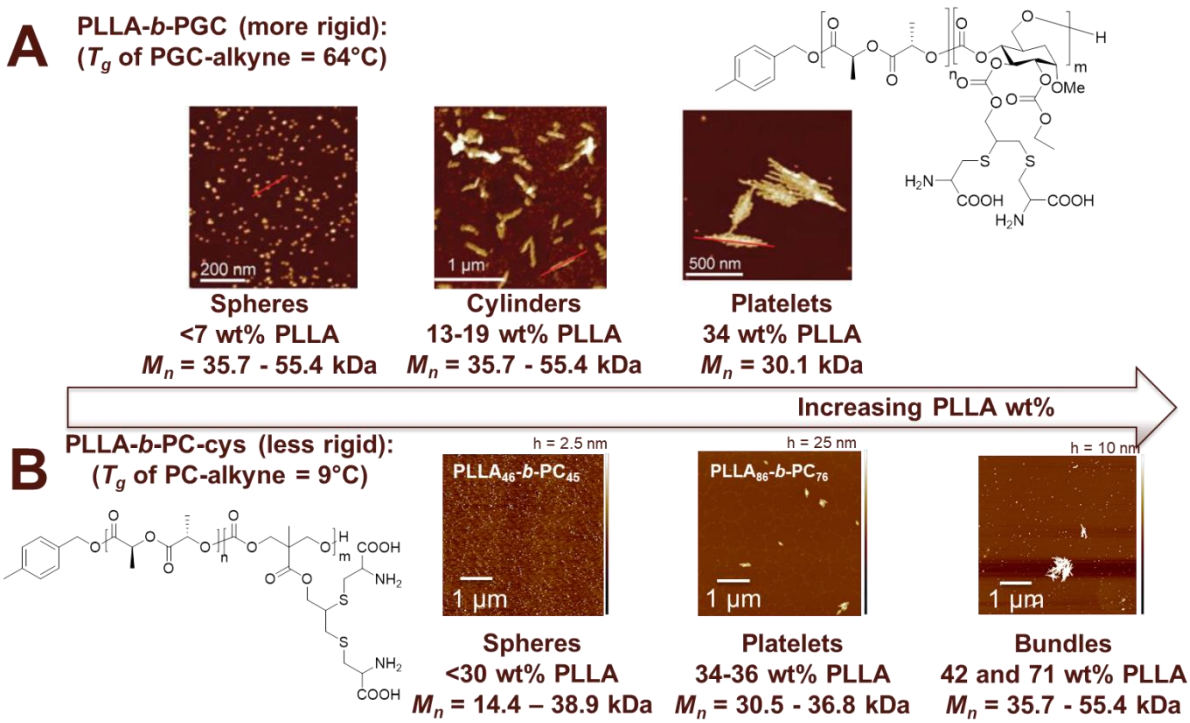

Figure 19. Comparison of the CDSA of PLLA-based block polymers: the higher-T_g polyglucose carbonates[12] *vs.* the lower-T_g aliphatic polycarbonates presented in this thesis. From the more rigid PLLA-*b*-PGCs, spheres were formed at <7 wt% PLLA, cylinders formed from block polymers with 13-19% wt% PLLA, and platelets were formed at 34% wt PLLA.[12] The more flexible PLLA-*b*-PCs described in this thesis yielded spheres at <30 wt% PLLA, platelets at 34-36 wt% PLLA, and bundles above 42 wt% PLLA.

SUMMARY AND FUTURE WORK

CDSA of a series of fully hydrolytically-degradable amphiphilic block polymers, PLLA-*b*-PC-cys, generated diverse morphologies, ranging from spheres to cylinders to cylinder bundles. The materials were synthesized by ring-opening polymerization and thiol-yne click chemistry, then thoroughly characterized using NMR spectroscopy, IR spectroscopy, and SEC to determine the molar mass and composition of the polymers. Thermal properties were characterized and were consistent with NMR spectroscopy-determined compositions. T_gs were observed for the alkyne-functionalized polymers, whereas no T_g was observed for polymers after cysteine-functionalization, perhaps due to incorporation of water with the increased hydrophilicity of the polymers, thereby plasticizing the samples. The Flory-Fox equation was used to predict the T_g for the series of alkyne-functionalized polymers, with good agreement between the predicted and the observed T_gs. Furthermore, the T_gs were, as expected, lower for these aliphatic PLLA-*b*-PC-alkyne block polymers (T_g range from -4 to 22 °C), compared to the more rigid PLLA-*b*-PGC alkyne (T_g = 64°C). CDSA of these polymers in aqueous solution yielded spherical, cylindrical, or platelet-like morphologies, depending on the ratio of the hydrophobic block to the hydrophilic block. By AFM, polymers with <30% PLLA formed only spheres, whereas those with intermediate weight percentages (34-36% PLLA) yielded platelets with lengths of *ca.* 500 nm. Finally, the polymers with the highest weight percent PLLA (42% and 71%) formed large bundles of cylinders, *ca.* 500 nm or longer.

The work adds to the current knowledge of structures that can be produced by crystallization-driven self-assembly using a hydrolytically degradable backbone. Previous CDSA work in the Wooley laboratory involving the assembly of block polymers with a poly(L-

lactide) semi-crystalline hydrophobic block and a sugar-based hydrophilic block (PLLA-*b*-PGC) showed that spheres were formed with 7% or less weight of PLLA, cylinders formed with 13-19% weight of PLLA, and platelets were formed at 34% weight of PLLA.[12] Satisfyingly, this is consistent with the expected influence of the backbone rigidity – the weight percent necessary to attain cylinders was found to be lower for the more rigid poly(glucose carbonate) system than in the more flexible PLLA-*b*-PC-cys described in this thesis.

This materials platform is amenable for use in a variety of applications. Future directions include the application of these materials in interface-promoted assembly and disassembly for fabrication of hybrid nanostructures and for antimicrobial delivery for treatment of recurrent urinary tract infections. Given that one in five young adult women in the US experience recurrent UTIs, it is clear that the current regimen of oral antibiotics does not effectively eradicate the bacteria.[64] UTIs account for 7 million physician visits per year at a cost of 1 billion dollars.[65] Furthermore, each year in the United States, at least 2 million people become infected with antibiotic-resistant bacteria and at least 23,000 people die each year as a direct result of these infections.[66] The fully degradable polymers described in this thesis, capable of assembly into a variety of tunable nanostructures, are under investigation as part of an interdisciplinary effort that aims to treat UTI with a unique approach towards eradication of antibiotic-resistant bacteria. Due to poor patient adherence to prescribed therapies and over-prescription of antibiotics, bacteria have now developed immunity to common classes of antibiotics, leading to the rise of "superbugs." Efficient delivery of therapeutic nanoparticles holds great potential for minimizing the use of resistance-inducing antibiotics in the future. Elongated nanostructures are expected to enable multivalent binding to cells and thereby promote internalization of silver-carrying nanoparticles into the uroepithelium to eradicate chronically-resident bacteria.[67]

REFERENCES

1. Panyam, J.; Labhasetwar, V., Biodegradable nanoparticles for drug and gene delivery to cells and tissue. *Adv. Drug Delivery Rev.* **2003,** *55* (3), 329-347.

2. Pratt, R. C.; Nederberg, F.; Waymouth, R. M.; Hedrick, J. L., Tagging alcohols with cyclic carbonate: a versatile equivalent of (meth)acrylate for ring-opening polymerization. *Chemical Commun.* **2008,** (1), 114-116.

3. Geng, Y.; Dalhaimer, P.; Cai, S.; Tsai, R.; Tewari, M.; Minko, T.; Discher, D. E., Shape effects of filaments versus spherical particles in flow and drug delivery. *Nat. Nanotechnol.* **2007,** *2*, 249.

4. Zhang, K.; Rossin, R.; Hagooly, A.; Chen, Z.; Welch, M. J.; Wooley, K. L., Folate-mediated Cell Uptake of Shell-crosslinked Spheres and Cylinders. *J. Polym. Sci., Part A: Polym. Chem.* **2008,** *46* (22), 7578-7583.

5. Elsabahy, M.; Wooley, K. L., Design of polymeric nanoparticles for biomedical delivery applications. *Chem. Soc. Rev.* **2012,** *41* (7), 2545-2561.

6. Su, L.; Khan, S.; Fan, J.; Lin, Y.-N.; Wang, H.; Gustafson, T. P.; Zhang, F.; Wooley, K. L., Functional sugar-based polymers and nanostructures comprised of degradable poly(d-glucose carbonate)s. *Polym. Chem.* **2017,** *8* (10), 1699-1707.

7. Elzeny, H.; Zhang, F.; Ali, E. N.; Fathi, H. A.; Zhang, S.; Li, R.; El-Mokhtar, M. A.; Hamad, M. A.; Wooley, K. L.; Elsabahy, M., Polyphosphoester nanoparticles as biodegradable platform for delivery of multiple drugs and siRNA. *Drug Des., Dev. Ther.* **2017,** *11*, 483-496.

8. Lonnecker, A. T.; Lim, Y. H.; Wooley, K. L., Functional Polycarbonate of a d-Glucal-Derived Bicyclic Carbonate via Organocatalytic Ring-Opening Polymerization. *ACS Macro Lett.* **2017,** *6* (7), 748-753.

9. Lim, Y. H.; Tiemann, K. M.; Heo, G. S.; Wagers, P. O.; Rezenom, Y. H.; Zhang, S.; Zhang, F.; Youngs, W. J.; Hunstad, D. A.; Wooley, K. L., Preparation and in Vitro Antimicrobial Activity of Silver-Bearing Degradable Polymeric Nanoparticles of Polyphosphoester-block-Poly(l-lactide). *ACS Nano* **2015,** *9* (2), 1995-2008.

10. Petzetakis, N.; Dove, A. P.; O'Reilly, R. K., Cylindrical micelles from the living crystallization-driven self-assembly of poly(lactide)-containing block copolymers. *Chem. Sci.* **2011,** *2* (5), 955-960.

11. Yu, W.; Inam, M.; Jones, J. R.; Dove, A. P.; O'Reilly, R. K., Understanding the CDSA of poly(lactide) containing triblock copolymers. *Polym. Chem.* **2017,** *8* (36), 5504-5512.

12. Song, Y.; Chen, Y.; Su, L.; Li, R.; Letteri, R. A.; Wooley, K. L., Crystallization-driven assembly of fully degradable, natural product-based poly(l-lactide)-block-poly(α-d-glucose carbonate)s in aqueous solution. *Polymer* **2017,** *122*, 270-279.

13. Young, R. J., Lovell, P. A., *Introduction to Polymers*. 2 ed.; CRC Press, LLC: Boca Raton, Florida, 1991.

14. Pratt, R. C.; Lohmeijer, B. G. G.; Long, D. A.; Waymouth, R. M.; Hedrick, J. L., Triazabicyclodecene: A Simple Bifunctional Organocatalyst for Acyl Transfer and Ring-Opening Polymerization of Cyclic Esters. *J. Am. Chem. Soc.* **2006,** *128* (14), 4556-4557.

15. Zhang, L.; Pratt, R. C.; Nederberg, F.; Horn, H. W.; Rice, J. E.; Waymouth, R. M.; Wade, C. G.; Hedrick, J. L., Acyclic Guanidines as Organic Catalysts for Living Polymerization of Lactide. *Macromolecules* **2010,** *43* (3), 1660-1664.

16. Kiesewetter, M. K.; Shin, E. J.; Hedrick, J. L.; Waymouth, R. M., Organocatalysis: Opportunities and Challenges for Polymer Synthesis. *Macromolecules* **2010,** *43* (5), 2093-2107.

17. Olsén, P.; Odelius, K.; Albertsson, A.-C., Thermodynamic Presynthetic Considerations for Ring-Opening Polymerization. *Biomacromolecules* **2016,** *17* (3), 699-709.

18. Saiyasombat, W.; Molloy, R.; Nicholson, T. M.; Johnson, A. F.; Ward, I. M.; Poshyachinda, S., Ring strain and polymerizability of cyclic esters. *Polymer* **1998,** *39* (23), 5581-5585.

19. Duda, A.; Kowalski, A.; Penczek, S.; Uyama, H.; Kobayashi, S., Kinetics of the Ring-Opening Polymerization of 6-, 7-, 9-, 12-, 13-, 16-, and 17-Membered Lactones. Comparison of Chemical and Enzymatic Polymerizations. *Macromolecules* **2002,** *35* (11), 4266-4270.

20. Alemán, C.; Betran, O.; Casanovas, J.; Houk, K. N.; Hall, H. K., Thermodynamic Control of the Polymerizability of Five-, Six-, and Seven-Membered Lactones. *J. Org. Chem.* **2009,** *74* (16), 6237-6244.

21. Lohmeijer, B. G. G.; Pratt, R. C.; Leibfarth, F.; Logan, J. W.; Long, D. A.; Dove, A. P.; Nederberg, F.; Choi, J.; Wade, C.; Waymouth, R. M.; Hedrick, J. L., Guanidine and Amidine Organocatalysts for Ring-Opening Polymerization of Cyclic Esters. *Macromolecules* **2006,** *39* (25), 8574-8583.

22. Zhu, K. J.; Hendren, R. W.; Jensen, K.; Pitt, C. G., Synthesis, properties, and biodegradation of poly(1,3-trimethylene carbonate). *Macromolecules* **1991,** *24* (8), 1736-1740.

23. Tyler, B.; Gullotti, D.; Mangraviti, A.; Utsuki, T.; Brem, H., Polylactic acid (PLA) controlled delivery carriers for biomedical applications. *Adv. Drug Delivery Rev.* **2016,** *107*, 163-175.

24. Saini, P.; Arora, M.; Kumar, M. N. V. R., Poly(lactic acid) blends in biomedical applications. *Adv. Drug Delivery Rev.* **2016,** *107*, 47-59.

25. Sheikh, Z.; Najeeb, S.; Khurshid, Z.; Verma, V.; Rashid, H.; Glogauer, M., Biodegradable Materials for Bone Repair and Tissue Engineering Applications. *Materials* **2015,** *8* (9), 5273.

26. Vroman, I.; Tighzert, L., Biodegradable Polymers. *Materials* **2009,** *2* (2), 307.

27. van Dijk, M.; Rijkers, D. T. S.; Liskamp, R. M. J.; van Nostrum, C. F.; Hennink, W. E., Synthesis and Applications of Biomedical and Pharmaceutical Polymers via Click Chemistry Methodologies. *Bioconjugate Chem.* **2009,** *20* (11), 2001-2016.

28. C., K. H.; G., F. M.; Barry, S. K., Click Chemistry: Diverse Chemical Function from a Few Good Reactions. *Angew. Chem., Int. Ed.* **2001,** *40* (11), 2004-2021.

29. Bader, H., 23. The addition of thiolacetic acid to ethynylcarbinols and the conversion of the adducts into aldols and [small alpha][small beta]-unsaturated aldehydes. *J. Chem. Soc.* **1956,** (0), 116-121.

30. Bader, H.; Cross, L. C.; Heilbron, I.; Jones, E. R. H., 132. Researches on acetylenic compounds. Part XVIII. The addition of thiolacetic acid to acetylenic hydrocarbons. The conversion of monosubstituted acetylenes into aldehydes and 1 : 2-dithiols. *J. Chem. Soc.* **1949,** (0), 619-623.

31. Fairbanks, B. D.; Scott, T. F.; Kloxin, C. J.; Anseth, K. S.; Bowman, C. N., Thiol−Yne Photopolymerizations: Novel Mechanism, Kinetics, and Step-Growth Formation of Highly Cross-Linked Networks. *Macromolecules* **2009,** *42* (1), 211-217.

32. Ochiai, B.; Tomita, I.; Endo, T., Chemical Modification of NovelAlkyne-Containing Polymers Obtained by Radical Polymerization ofConjugated Enynes. *Polym. Bull.* **2004,** *51* (4), 263-269.

33. Eiichi, K.; Toshizumi, Y.; Sadahito, A.; Junji, F., Addition polymerization of 2- cyano-1, 4- benzenedithiol to 1,4- diethynylbenzene and properties of polymers. *J. Polym. Sci., Part A: Polym. Chem.* **1995,** *33* (14), 2403-2414.

34. Shiro, M., The effect of pressure and temperature on the specific volume of polyethylene. *J. Polym. Sci.* **1962,** *57* (165), 569-588.

35. Heimenz, P. C., Lodge, Timothy P., Glass Transition. In *Polym. Chem.*, 2nd ed.; CRC Press: Boca Raton, FL, 2007; pp 465-509.

36. Daimon, H.; Okitsu, H.; Kumanotani, J., Glass Transition Behaviors of Random and Block Copolymers and Polymer Blends of Styrene and Cyclododecyl Acrylate. I. Glass Transition Temperatures. *Polymer Journal* **1975,** *7*, 460.

37. Chitoshi, N.; Shin- ya, T., Glass transition and mechanical properties of PLLA and PDLLA- PGA copolymer blends. *J. Appl. Polym. Sci.* **2004,** *93* (5), 2164-2173.

38. Mai, Y.; Eisenberg, A., Self-assembly of block copolymers. *Chem. Soc. Rev.* **2012,** *41* (18), 5969-5985.

39. Hayward, R. C.; Pochan, D. J., Tailored Assemblies of Block Copolymers in Solution: It Is All about the Process. *Macromolecules* **2010,** *43* (8), 3577-3584.

40. Du, J.; O'Reilly, R. K., Advances and challenges in smart and functional polymer vesicles. *Soft Matter* **2009,** *5* (19), 3544-3561.

41. Crassous, J. J.; Schurtenberger, P.; Ballauff, M.; Mihut, A. M., Design of block copolymer micelles via crystallization. *Polymer* **2015,** *62*, A1-A13.

42. He, X.; He, Y.; Hsiao, M.-S.; Harniman, R. L.; Pearce, S.; Winnik, M. A.; Manners, I., Complex and Hierarchical 2D Assemblies via Crystallization-Driven Self-Assembly of Poly(l-lactide) Homopolymers with Charged Termini. *J. Am. Chem. Soc.* **2017,** *139* (27), 9221-9228.

43. Gilroy, J. B.; Gädt, T.; Whittell, G. R.; Chabanne, L.; Mitchels, J. M.; Richardson, R. M.; Winnik, M. A.; Manners, I., Monodisperse cylindrical micelles by crystallization-driven living self-assembly. *Nat. Chem.* **2010,** *2*, 566.

44. Schmelz, J.; Karg, M.; Hellweg, T.; Schmalz, H., General Pathway toward Crystalline-Core Micelles with Tunable Morphology and Corona Segregation. *ACS Nano* **2011,** *5* (12), 9523-9534.

45. Schmelz, J.; Schedl, A. E.; Steinlein, C.; Manners, I.; Schmalz, H., Length Control and Block-Type Architectures in Worm-like Micelles with Polyethylene Cores. *J. Am. Chem. Soc.* **2012,** *134* (34), 14217-14225.

46. Gwyther, J.; Gilroy Joe, B.; Rupar Paul, A.; Lunn David, J.; Kynaston, E.; Patra Sanjib, K.; Whittell George, R.; Winnik Mitchell, A.; Manners, I., Dimensional Control of Block Copolymer Nanofibers with a π- Conjugated Core: Crystallization- Driven Solution Self-Assembly of Amphiphilic Poly(3- hexylthiophene)- b- poly(2- vinylpyridine). *Chem. - Eur. J.* **2013,** *19* (28), 9186-9197.

47. Qian, J.; Li, X.; Lunn, D. J.; Gwyther, J.; Hudson, Z. M.; Kynaston, E.; Rupar, P. A.; Winnik, M. A.; Manners, I., Uniform, High Aspect Ratio Fiber-like Micelles and Block Co-micelles with a Crystalline π-Conjugated Polythiophene Core by Self-Seeding. *J. Am. Chem. Soc.* **2014,** *136* (11), 4121-4124.

48. Ogi, S.; Stepanenko, V.; Sugiyasu, K.; Takeuchi, M.; Würthner, F., Mechanism of Self-Assembly Process and Seeded Supramolecular Polymerization of Perylene Bisimide Organogelator. *J. Am. Chem. Soc.* **2015,** *137* (9), 3300-3307.

49. Ogi, S.; Sugiyasu, K.; Manna, S.; Samitsu, S.; Takeuchi, M., Living supramolecular polymerization realized through a biomimetic approach. *Nat. Chem.* **2014,** *6*, 188.

50. Xiaojie, M.; Yibin, Z.; Yifan, Z.; Yin, L.; Yanke, C.; Jincai, Z., Fabrication of Chiral-Selective Nanotubular Heterojunctions through Living Supramolecular Polymerization. *Angew. Chem., Int. Ed.* **2016,** *55* (33), 9539-9543.

51. Zhang, W.; Jin, W.; Fukushima, T.; Mori, T.; Aida, T., Helix Sense-Selective Supramolecular Polymerization Seeded by a One-Handed Helical Polymeric Assembly. *J. Am. Chem. Soc.* **2015,** *137* (43), 13792-13795.

52. Zhang, W.; Jin, W.; Fukushima, T.; Saeki, A.; Seki, S.; Aida, T., Supramolecular Linear Heterojunction Composed of Graphite-Like Semiconducting Nanotubular Segments. *Science* **2011,** *334* (6054), 340-343.

53. Boott, C. E.; Gwyther, J.; Harniman, R. L.; Hayward, D. W.; Manners, I., Scalable and uniform 1D nanoparticles by synchronous polymerization, crystallization and self-assembly. *Nat. Chem.* **2017,** *9*, 785.

54. Hudson, Z. M.; Lunn, D. J.; Winnik, M. A.; Manners, I., Colour-tunable fluorescent multiblock micelles. *Nat. Commun.* **2014,** *5*, 3372.

55. Wang, X.; Guerin, G.; Wang, H.; Wang, Y.; Manners, I.; Winnik, M. A., Cylindrical Block Copolymer Micelles and Co-Micelles of Controlled Length and Architecture. *Science* **2007,** *317* (5838), 644-647.

56. Gädt, T.; Ieong, N. S.; Cambridge, G.; Winnik, M. A.; Manners, I., Complex and hierarchical micelle architectures from diblock copolymers using living, crystallization-driven polymerizations. *Nat. Mater.* **2009,** *8*, 144.

57. He, F.; Gädt, T.; Manners, I.; Winnik, M. A., Fluorescent "Barcode" Multiblock Co-Micelles via the Living Self-Assembly of Di- and Triblock Copolymers with a Crystalline Core-Forming Metalloblock. *J. Am. Chem. Soc.* **2011,** *133* (23), 9095-9103.

58. Qiu, H.; Cambridge, G.; Winnik, M. A.; Manners, I., Multi-Armed Micelles and Block Co-micelles via Crystallization-Driven Self-Assembly with Homopolymer Nanocrystals as Initiators. *J. Am. Chem. Soc.* **2013,** *135* (33), 12180-12183.

59. Rupar, P. A.; Chabanne, L.; Winnik, M. A.; Manners, I., Non-Centrosymmetric Cylindrical Micelles by Unidirectional Growth. *Science* **2012,** *337* (6094), 559-562.

60. Södergård, A.; Stolt, M., Properties of lactic acid based polymers and their correlation with composition. *Prog. Polym. Sci.* **2002,** *27* (6), 1123-1163.

61. Cysteine from Wacker. https://www.wacker.com/cms/en/products/product_groups/cystein.jsp (accessed May 12).

62. Simón, L.; Goodman, J. M., The Mechanism of TBD-Catalyzed Ring-Opening Polymerization of Cyclic Esters. *J. Org. Chem.* **2007,** *72* (25), 9656-9662.

63. Sun, L.; Petzetakis, N.; Pitto-Barry, A.; Schiller, T. L.; Kirby, N.; Keddie, D. J.; Boyd, B. J.; O'Reilly, R. K.; Dove, A. P., Tuning the Size of Cylindrical Micelles from Poly(l-lactide)-b-poly(acrylic acid) Diblock Copolymers Based on Crystallization-Driven Self-Assembly. *Macromolecules* **2013,** *46* (22), 9074-9082.

64. Tolkoff-Rubin, N. E., Cotran, R. S., Rubin, R. H. , Urinary tract infection, pyelonephritis, and reflux nephropathy. In *Brenner & Rector's The Kidney.* , 8th ed.; Brenner, B. M., Ed. Saunders: Philadelphia, 2008; Vol. 2, pp 1203–1238.

65. Nickel, J. C., Practical Management of Recurrent Urinary Tract Infections in Premenopausal Women. *Reviews in Urology* **2005,** *7* (1), 11-17.

66. Antibiotic Resistance Threats in the United States, 2013. . https://www.cdc.gov/drugresistance/pdf/ar-threats-2013-508.pdf (accessed Jan 11, 2017).

67. Geng, Y.; Dalhaimer, P.; Cai, S.; Tsai, R.; Tewari, M.; Minko, T.; Discher, D. E., Shape effects of filaments versus spherical particles in flow and drug delivery. *Nature Nanotechnology* **2007,** *2*, 249.

APPENDIX

Characterization of polymers using molar mass and degree of polymerization

One of the ways that polymers can be characterized by molar mass and degree of polymerization. The molar mass of a homopolymer $M = xM_0$, where M is the molar mass, x is the number of repeat units, and M_0 is the weight of each repeat unit. Since the molar mass is discontinuous – *i.e.* not a discrete value – the molar mass is typically described by a distribution curve. The molar mass averages that are important to this project are the number-average molar mass, and the weight-average molar mass. The number average molecular mass is defined as the sum of the products of the molar mass of each fraction, multiplied by its mole fraction, or $M_n = \Sigma X_i M_i$, where X_i is the mole fraction of molecules of molar mass M_i, and M_i is the ratio of N_i to the total number of molecules. The weight average molecular mass is the sum of the products of the molar mass of each fraction multiplied by its weight fraction, or $M_w = \Sigma w_i M_i$, where w_i is the mass of molecules of molar mass M_i, divided by the total mass of all the molecules present. The ratio M_w / M_n is known as the dispersity of the polymer, $Đ$. It is often used as a measure of the breadth of the molar mass distribution. Typically, polymers have a range between $Đ$ = 1.5-2.0, while controlled polymerizations yield polymers with $Đ$ < 1.2. A perfectly monodisperse polymer would have $Đ$ = 1.00.

Step growth *vs.* chain growth polymers

Syntheses of polymers have two different types – step growth and chain growth. In step growth polymerization, the polymer chains grow between any two molecular species. The degree of polymerization is related by the Carother's equation, $x_n = (1\text{-}p)^{-1}$, where x_n is the average degree of polymerization, and p is the fraction of reactive group conversion. Conversely, in chain growth polymerization, the polymer chains grow only by reaction of

monomer on the active chain end. Chain growth polymerization requires an initiator, which starts the growth of the chain. Chain growth polymerizations have three distinct steps: initiation, during which active chain ends are generated, propagation, during which polymerization occurs, and termination, during which the active chain end is quenched. Chain growth polymerization can be categorized into three groups, depending on the nature of the reactive chain end species: anionic, cationic, and free radical.[13]

FTIR spectra for the post-polymerization functionalization with cysteine

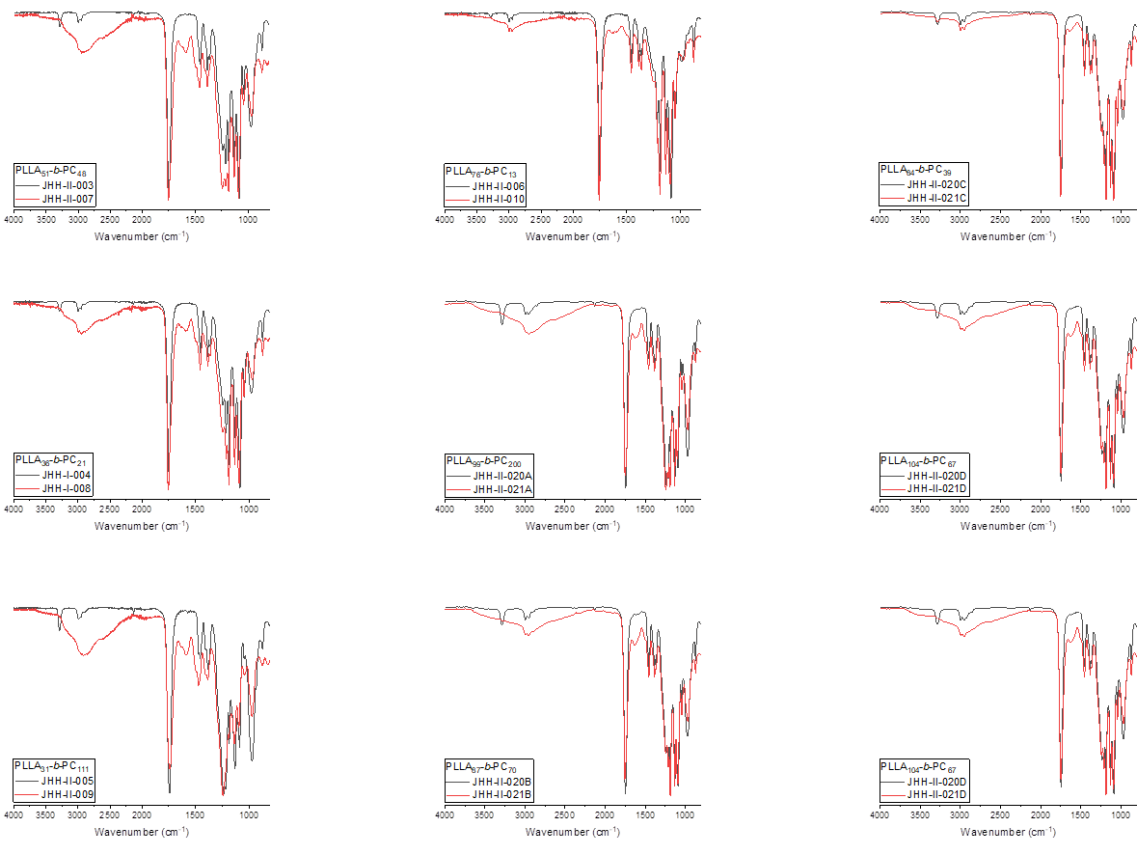

Figure 20. Additional FTIR spectra for the post-polymerization functionalization with cysteine

AFM height images of PLLA-*b*-PC-cys

Ratio of n : m:	**1 : 2.1**	**1 : 1.6**	**1 : 1.5**
Wt% of PLLA:	**18.0%**	**21.6%**	**12.7%**
Resulting height:	**2 ± 1 nm**	**1 ± 1 nm**	**2 ± 1 nm**

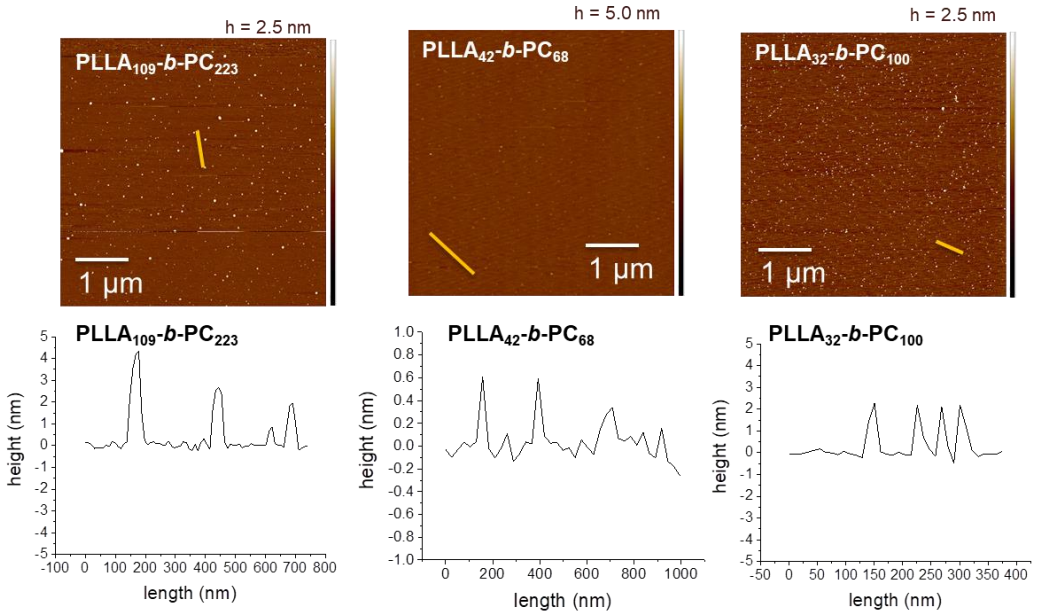

Ratio of n : m:	**1 : 1**	**1.1 : 1**	**1.2 : 1**
Wt% PLLA:	**31.7%**	**33.7%**	**35.6%**
Resulting height:	**9 ± 2 nm**	**16 ± 5 nm**	**10 ± 3 nm**

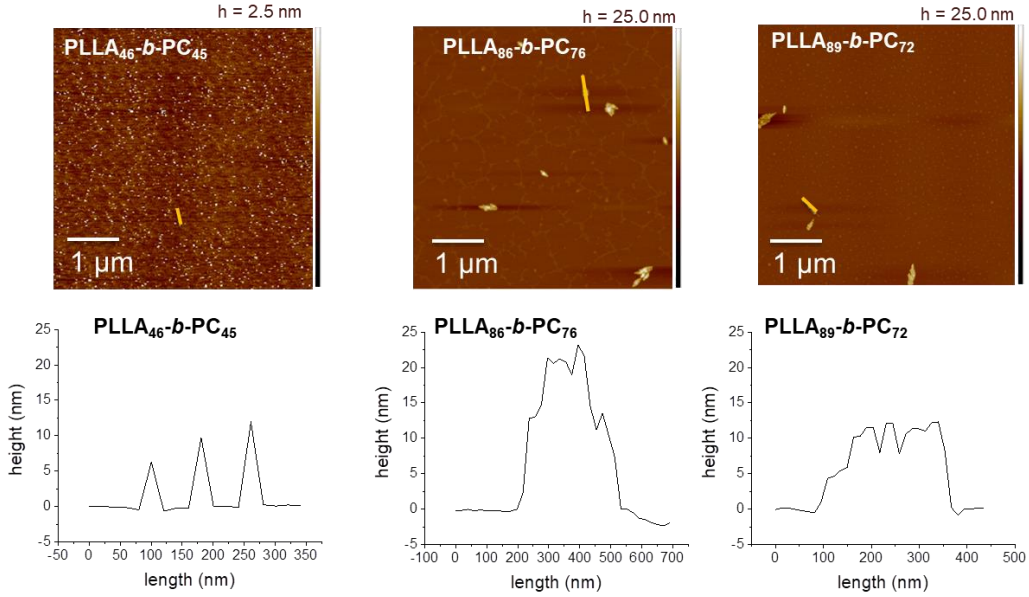

Ratio of n : m:	**1.7 : 1**	**2.1 : 1**	**6.3 : 1**
Wt% PLLA:	**42.8%**	**49.1%**	**71.2%**
Resulting height:	**10 ± 3 nm**	**14 ± 4 nm**	**10 ± 2 nm**

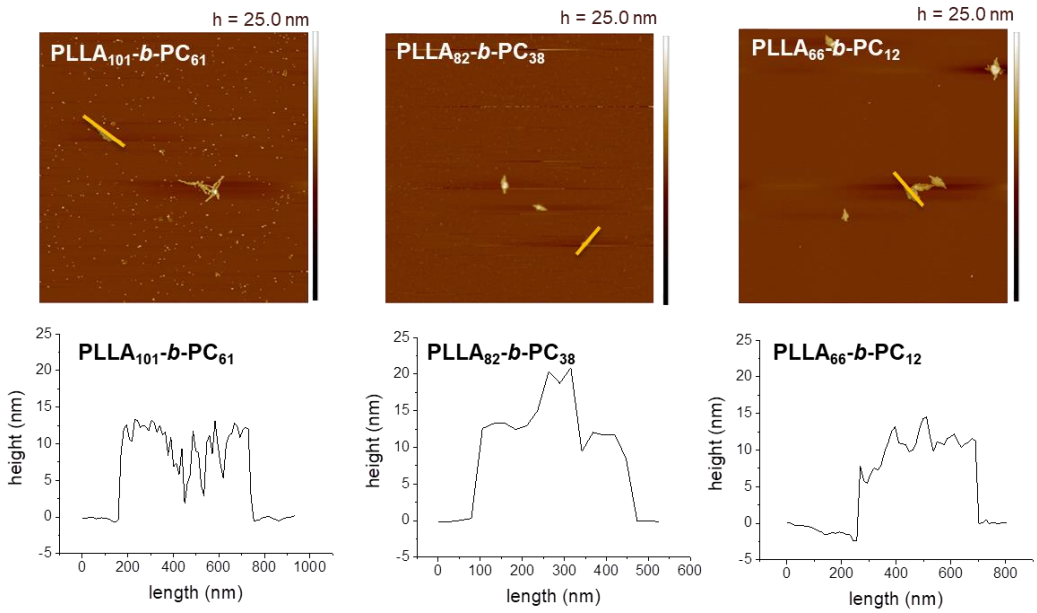

Figure 21. AFM images of PLLA-*b*-PC-cys, with a yellow line indicating where height profile was taken.

DSC traces for the post-polymerization functionalization with cysteine

$PLLA_{46}$-*b*-PC_{45} (1 : 1)

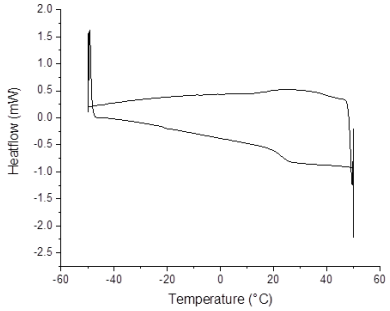

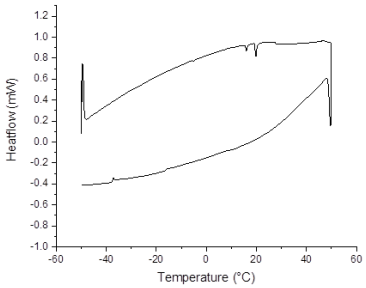

$PLLA_{32}$-*b*-PC_{100} (1 : 1.5)

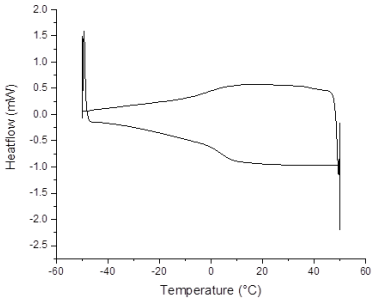

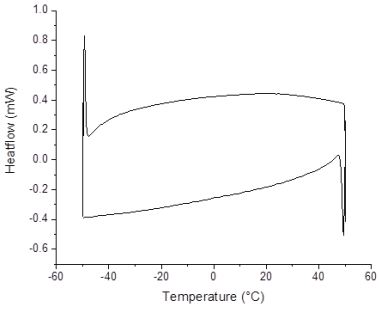

$PLLA_{42}$-*b*-PC_{68} (1 : 1.6)

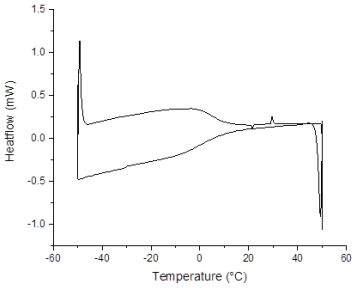

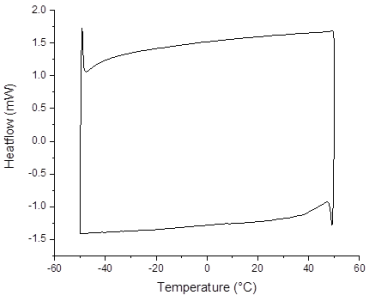

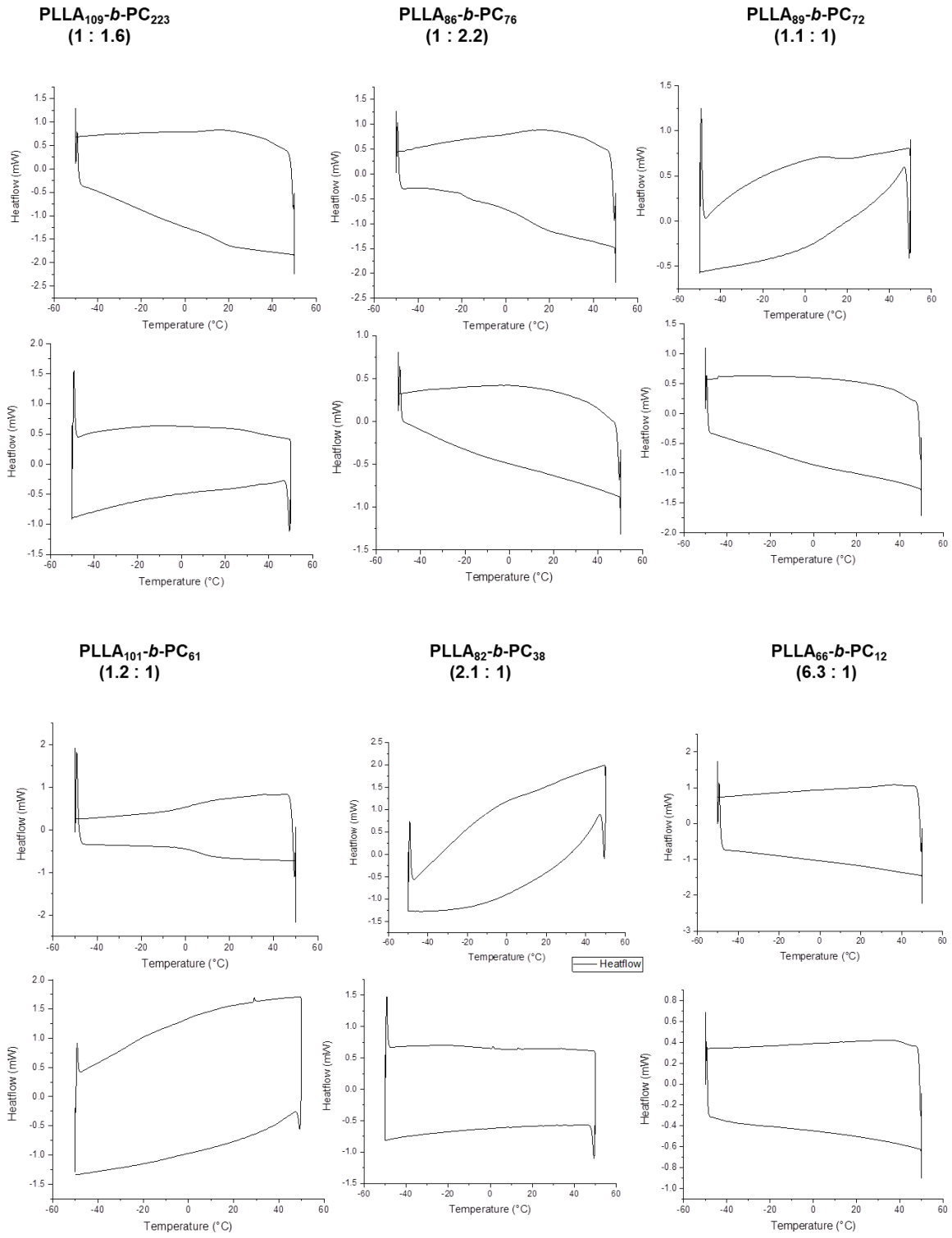

Figure 22. DSC data of all samples. The top curve is the PLLA-*b*-PC-alkyne, while the bottom curve is the PLLA-*b*-PC-cys. The heating traces are on the bottom of each curve and the cooling traces on the top.

Additional AFM images

Degree of polymerization (ratio of n:m) :

$PLLA_{46}$-*b*-PC_{45} (1 : 1):

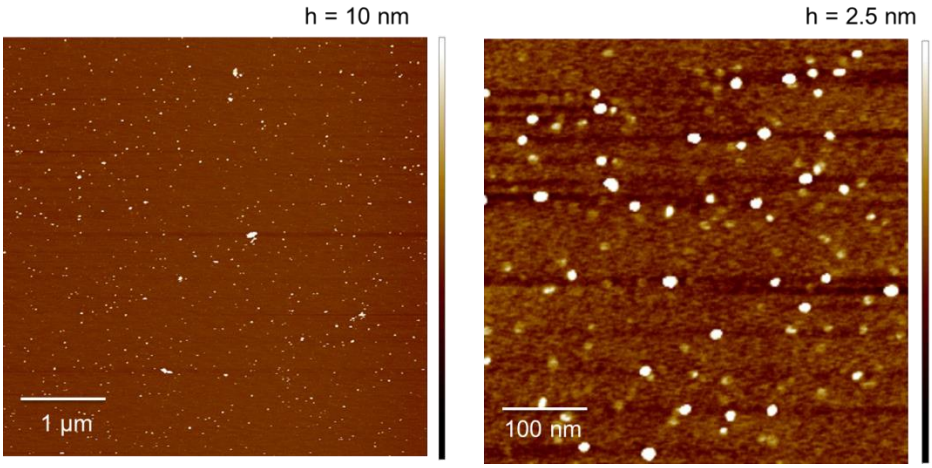

$PLLA_{66}$-*b*-PC_{100} (1 : 1.5):

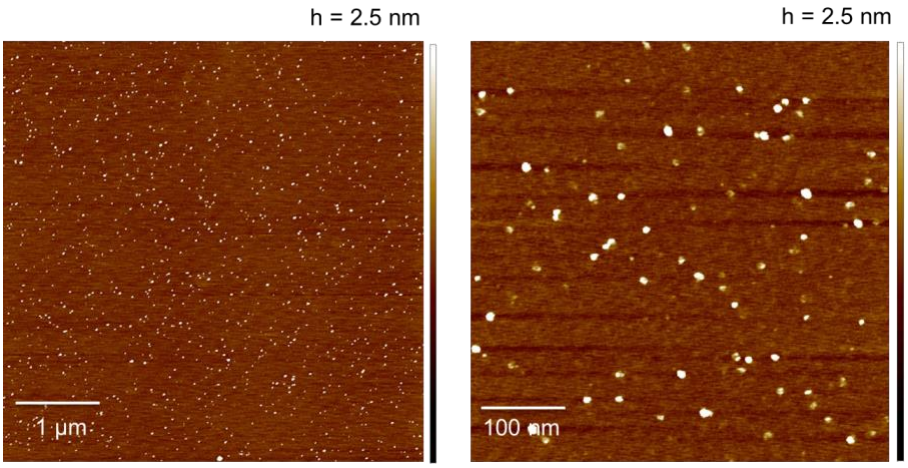

$PLLA_{42}$-*b*-PC_{68} (1 : 1.6):

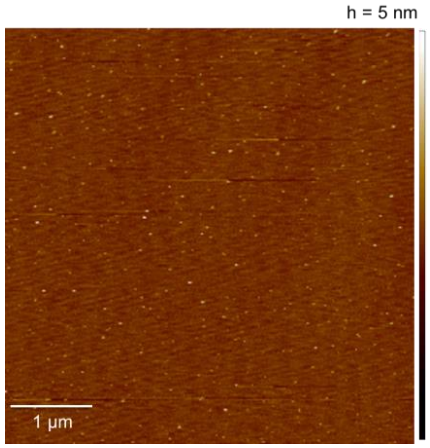

PLLA$_{109}$-*b*-PC$_{223}$ (1 : 2.2):

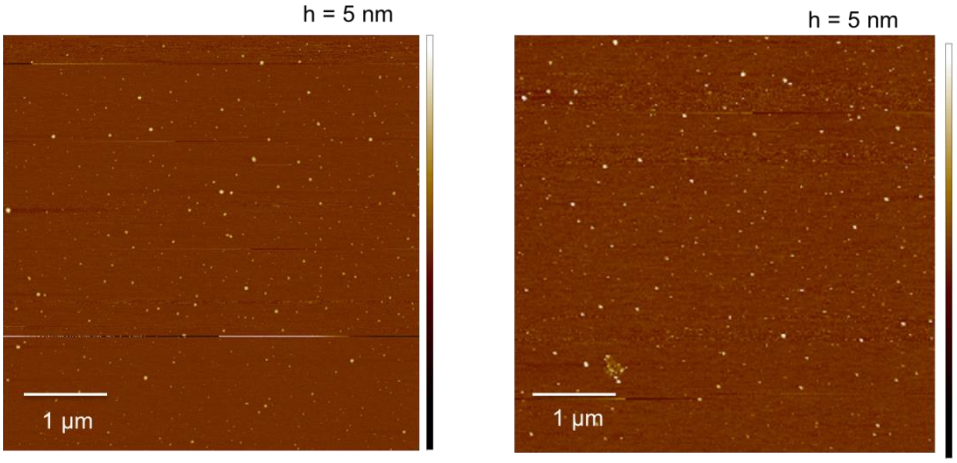

PLLA$_{86}$-*b*-PC$_{76}$ (1.1 : 1):

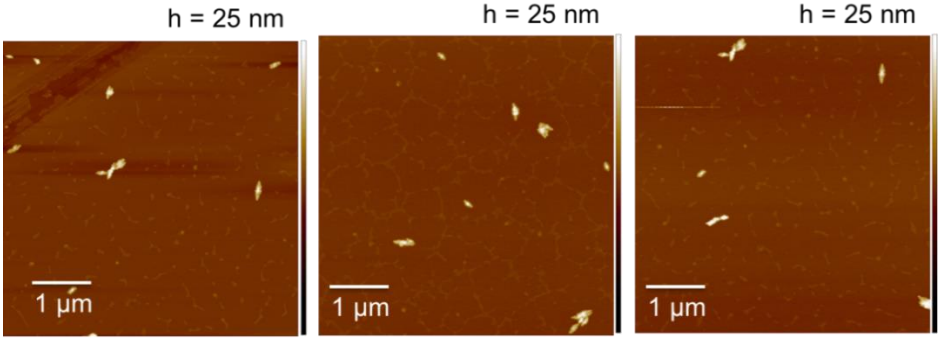

PLLA$_{89}$-*b*-PC$_{72}$ (1.2 : 1):

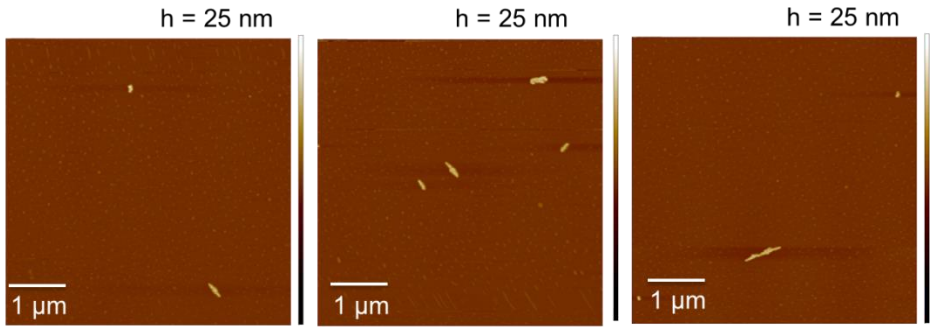

PLLA$_{82}$-*b*-PC$_{38}$ (2.1 : 1)

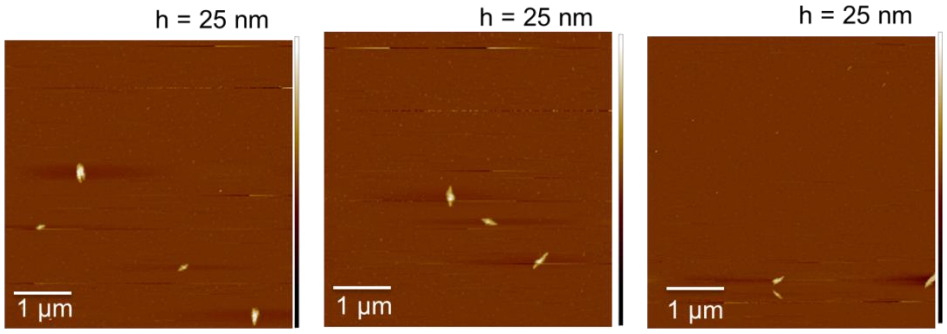

PLLA$_{66}$-*b*-PC$_{12}$ (6.3 : 1):